EVALUATION AND SIMULATION OF NEMS CANTILEVER RELAYS

THESIS

Presented to the Graduate Council of
Texas State University-San Marcos
in Partial Fulfillment
of the Requirements

for the Degree

Master of SCIENCE

by

Jason Williams, B.S.

San Marcos, Texas
August 2010

ACKNOWLEDGEMENTS

I would like to thank SEMATECH for supplying me with samples and electrical data for my study. I would like to thank Casey Smith, Carl Ventrice, Gregory Spencer, and Anup Bandyopadhyay for their training and guidance given to me during my time at Texas State University-San Marcos. I would like to thank NSF IGERT 0549487 and DMR 0421404 for helping to support my research here at Texas State University-San Marcos.

I would also like to thank Team Calculus and the rest of my fellow physics students for their support and entertainment during my studies. I would also like to thank Dr. Ventrice and Dr. Smith for being on my committee. I would also like to thank Dr. Ventrice for always being available to answer questions and help out.

This manuscript was submitted on May 4, 2010.

TABLE OF CONTENTS

LIST OF FIGURES

LIST OF TABLES

ABSTRACT

EVALUATION AND SIMULATION OF NEMS CANTILEVER RELAYS

by

Jason Williams, B.S.

Texas State University-San Marcos

SUPERVISING PROFESSOR: GREGORY SPENCER

Electrostatically-actuated NEMS cantilevers were fabricated for testing as a potential replacement for nanoscale circuit components in power-critical applications such as spacecraft. These cantilevers are manipulated and switched in a horizontal plane by applying a voltage to lateral electrodes. A variety of poly-Si cantilevers were fabricated at SEMATECH with a range of beam lengths (from 2 μm to 14 μm) and electrode gap spacing (from 110 nm to 140 nm). After fabrication, the cantilevers were tested at SEMATECH to determine the voltage required to generate sufficient electrostatic force between the driving electrode and beam to bring the beam into contact with the collector. This pull-in voltage was measured as a function of device dimensions. To simulate the device operation, a model was created in COMSOL, a NEMS simulation software package. Simulations of pull-in voltage and pull-in time were compared to the data to both validate the model and estimate the frequency response of the devices. Variations of model device parameters such as beam thickness, height, gap size, and

Young's modulus were used to define a design space based on power requirements. SEM images were obtained at Texas State University-San Marcos to study failure mechanisms of various tested devices. This work is systematically evaluating the effects of device dimensions on the operational characteristics and failure mechanisms of lateral nanoscale cantilevers for low power applications.

CHAPTER 1

INTRODUCTION

A recent trend in the semiconductor industry has been the study of nano-electro-mechanical systems (NEMS).[1] The primary reason for this interest in studying NEMS is because of the ability to integrate them with conventional CMOS microchips. They also have various properties that can be used to solve unique problems. One of the problems that NEMS may be able to solve is the excess power consumption in some conventional transistor-based logic devices. Because of quantum mechanical tunneling, field-effect transistors (FETs) with gate oxides thinner than 2 nm have a leakage current that is drawn across the gate oxide when it is biased, which leads to a loss of available power. In addition, there is a small leakage current in the off-state of FETs. In contrast, due to a lack of a physical connection in a NEMS cantilever in the off-state, there will be a much lower leakage current as compared to an FET. Therefore, NEMS cantilevers are being studied as a viable replacement for transistors in some situations. In other words, mechanical switches could possibly replace electrical switches for applications where power consumption is the primary concern.

The NEMS cantilever structure works by using Coulomb attraction to actuate the cantilever, which either makes or breaks a physical connection that allows or prevents current from flowing through the device. This property enables it to be used as a logic element. Just like in transistors, there is a high current in the on-state and that high current can be used to represent a one, and can be the off-state there is a low current that is used to represent a zero.

In this study, the NEMS cantilever consists of four terminals: the cantilever, the cantilever contact, and the two driving electrodes, as seen in Fig. 1.1. The various design parameters that effect the operation of the device are the width of the cantilever w_{cant}, the vertical thickness of the device t, the length of the cantilever l_{cant}, the gap between the electrode and the cantilever g_{elect}, and the gap between the cantilever contact and the cantilever g_{cont}. These various parameters can be seen in Fig. 1.1, except for the thickness, which would be coming out of the page.

A good comparison for the physics behind the operation of this device is to model it as a parallel plate capacitor being held apart by a spring, as shown in Fig. 1.2.[2] The gap size of the capacitor g is equal to the initial gap size g_0 minus the distance the plate has

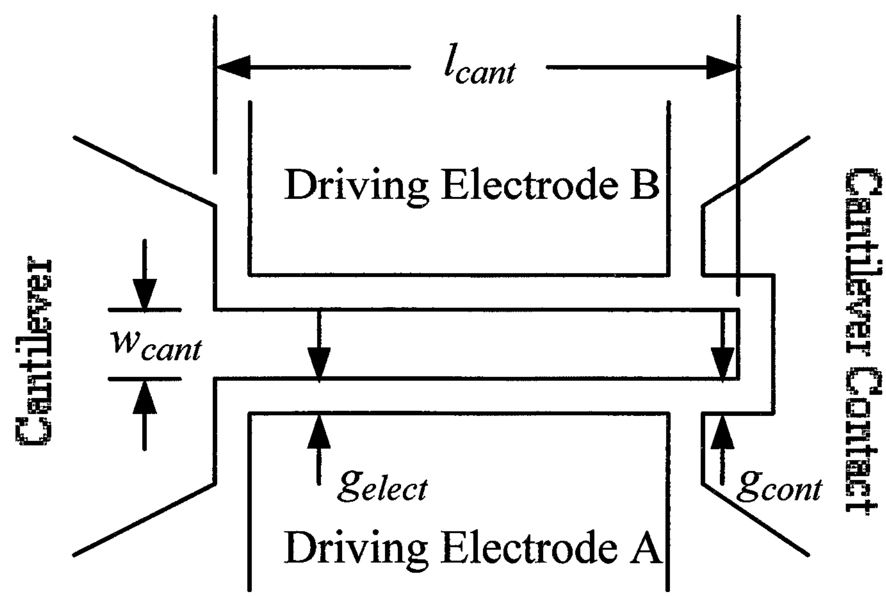

Fig. 1.1: Schematic of cantilever structure.

traveled z:

$$g = g_0 - z \; . \qquad [1]$$

Using Hooks law the displacement z as a function of force F and spring constant k is found

$$z = \frac{F}{k} \; . \qquad [2]$$

Equation 1 now becomes

$$g = g_0 - \frac{F}{k} \; . \qquad [3]$$

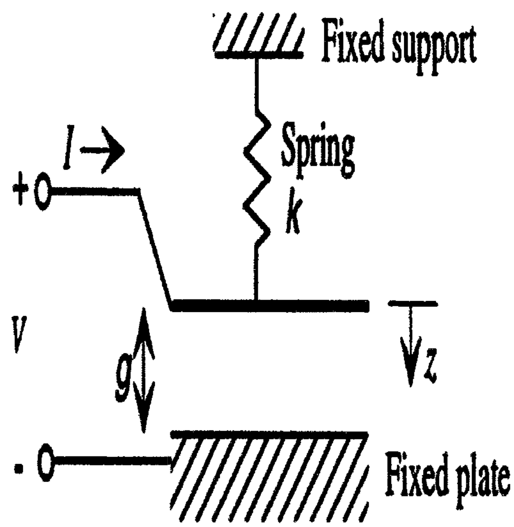

Fig. 1.2: Schematic of capacitor structure.[3]

Since the energy stored in the capacitor depends on both the charge stored and the gap, a two port capacitor model is used to describe the device as seen in Fig. 1.3.

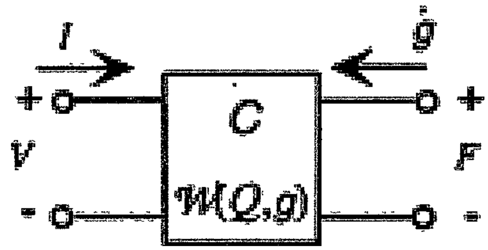

Fig. 1.3: Schematic of two-port capacitor.[4]

The energy stored in a capacitor is given by

$$W = \frac{1}{2} g V^2 = \frac{1}{2} \frac{Q^2}{2C} . \qquad [4]$$

Since the capacitance of a parallel plate capacitor is given by

$$C = \frac{\varepsilon A}{g} , \qquad [5]$$

the energy stored can be written as

$$W(Q,g) = \frac{Q^2 g}{2\varepsilon A} . \qquad [6]$$

This leads to the equations for force and for voltage:

$$F = \left. \frac{\partial W(Q,g)}{\partial g} \right|_Q = \frac{Q^2}{2\varepsilon A} , \qquad [7]$$

$$V = \left. \frac{\partial W(Q,g)}{\partial Q} \right|_g = \frac{Qg}{\varepsilon A} . \qquad [8]$$

By substituting Eqns. 7 and 8 into Eqn. 3, an equation for the gap size as a function of applied voltage is obtained

$$g = g_0 - \frac{\varepsilon A}{2kg^2} V^2 . \qquad [9]$$

Equation 9 can be used as an analog for the cantilever design since it has an identical initial force. However, since the cantilever is bending instead of moving uniformly, as is the case in the parallel plate capacitor, the force does not scale at the same rate. This equation though, will give the proportionality of the design parameters for the cantilever and provide an idea of how the device will operate.

To understand how the spring constant of the cantilever changes with the variation of the design parameters, an equation for the beam deflection as a function of those parameters is needed.[5] The moment equation for the cantilever beam is given by

$$M(x) = -\frac{1}{2}qx^2, \tag{10}$$

where $q = F/l$ is the force per unit length and x is the distance from the free end of the cantilever. The moment equation can also be written as

$$M(x) = EIv''(x), \tag{11}$$

where E is the Young's modulus, v'' is the curvature of deflection, and I is the area moment of inertia, which is given by

$$I = \frac{1}{12}bh^3, \tag{12}$$

b is the vertical thickness of the cantilever, and h is the width of the cantilever. As schematic of a cantilever with a uniform force load q is given in Fig. 1.4.

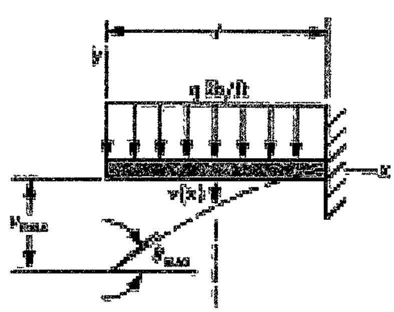

Fig. 1.4: Schematic of beam structure.[6]

The rigid connection at the base of the cantilever beam leads to boundary conditions

$$v'(l) = 0 \qquad [13]$$

and

$$v(l) = 0, \qquad [14]$$

where v' is the slope and v is the deflection. Integration of equation 10 leads to

$$v(x) = -\frac{q}{24EI}(x^4 - 4l^3x + 3l^4), \qquad [15]$$

where l is the length of the cantilever. From this equation, the maximum deflection of the beam is obtained

$$v_{\max} = -\frac{ql^4}{8EI}. \qquad [16]$$

By using v_{max} as z in equation 2 and performing a few algebraic manipulations, an equation for the spring constant as a function of the design parameters is obtained

$$k = \frac{2Ebh^3}{3l^3}. \qquad [17]$$

Therefore, the pull-in voltage should decrease as the length of the cantilever increases since the spring constant decreases as the inverse cube of the cantilever length.

There are several considerations that must be addressed before NEMS cantilevers can be used for practical logic devices. For instance, problems with contact resistance in current cantilever designs result in excessive power loss and cantilever failure. To address this issue, the use of a mercury contact to lower the power loss in the on-state has been studied.[7] Also thermal effects during the packaging of the devices can cause device failure.[8] The switching speed of conventional poly-Si cantilevers is much slower than what is needed to compete with conventional FET-based logic devices. To address this issue, ultra-high speed switches using piezoelectric actuation have been proposed.[9] There are also various options for the design of the cantilever that could be used for logic applications. In order to investigate the possibility of using some of these designs simulations of various beam dimensions have been studied to determine their pull-in voltage and natural frequencies.[10]

From an operational standpoint there are two important factors in the usability of these cantilevers as logic devices. First is the pull-in voltage since these devices are intended to be integrated with other CMOS technology, the actuation voltage would ideally be equivalent to the voltages already used by other components on the chip. Second is the speed at which the cantilevers connect. The speed at which these cantilevers will make or break contact has a direct correlation to the speed of the computations. Both of these factors are investigated in this study as well as various failure mechanisms of the device and the effects of changing design parameters on the pull-in voltage.

CHAPTER 2

DEVICES AND PROCEDURE

Device Design and Process Flow

The design of the cantilever structure was performed at Stanford University, and the cantilever arrays were fabricated at SEMATECH in Austin. There were nine wafers containing cantilever arrays with cantilever lengths ranging from l_{cant} = 2 μm up to l_{cant} = 14 μm. The electrode gap g_{elect} ranges from 110 up to 150 nm in 10 nm steps. The width of the cantilever w_{cant} and the contact gap g_{cont} are 10 nm less then g_{elect}. The thickness of the cantilever t is 200 nm for all the devices. The cantilevers are grown on a sacrificial layer of SiO_2, which allows the cantilever beam to be released from the substrate using an anhydrous (no water) vapor HF etch. The wafers 1, 2, and 3 had a sacrificial layer of 400 nm, the next set of wafers 4, 5, and 6 had a sacrificial layer of 600 nm and the last three wafers 7, 8, and 9 had a sacrificial layer of 800 nm. Wafers 1, 4, and 7 were implanted with 12 keV boron ions with a fluence of 8.5×10^{14} cm^{-2}. Wafers 2, 5, 8 were implanted with 15 keV boron ions with a fluence of 1×10^{16} cm^{-2}. Wafers 3, 6, and 9 were implanted with 60 keV arsenic ions with a fluence of 8.5×10^{14} cm^{-2}.

The following generalized procedure was used to create the samples. First a sacrificial layer was grown onto a (100) wafer followed by a structural poly-Si layer. This structural layer was then patterned and etched. After the structures were created, an addition of a titanium nitride sidewall was done through selective patterning. Trenches were then created in the sacrificial layer, and finally the sacrificial layer was etched out using an anhydrous vapor HF. See Fig. 2.1 provided by SEMATECH for a generalized process flow chart. After all of the processing is completed, the devices are no longer at the exact same scale as they were drawn. There are proximity effects during the photo lithography (due to diffraction) that can cause regions to either over or under expose. The etching process can result in the formation of non-uniform sidewalls. In addition, the growth of the TiN coating on the sidewalls results in a reduction of the gap sizes. The samples investigated in this study were produced and owned by SEMATECH.

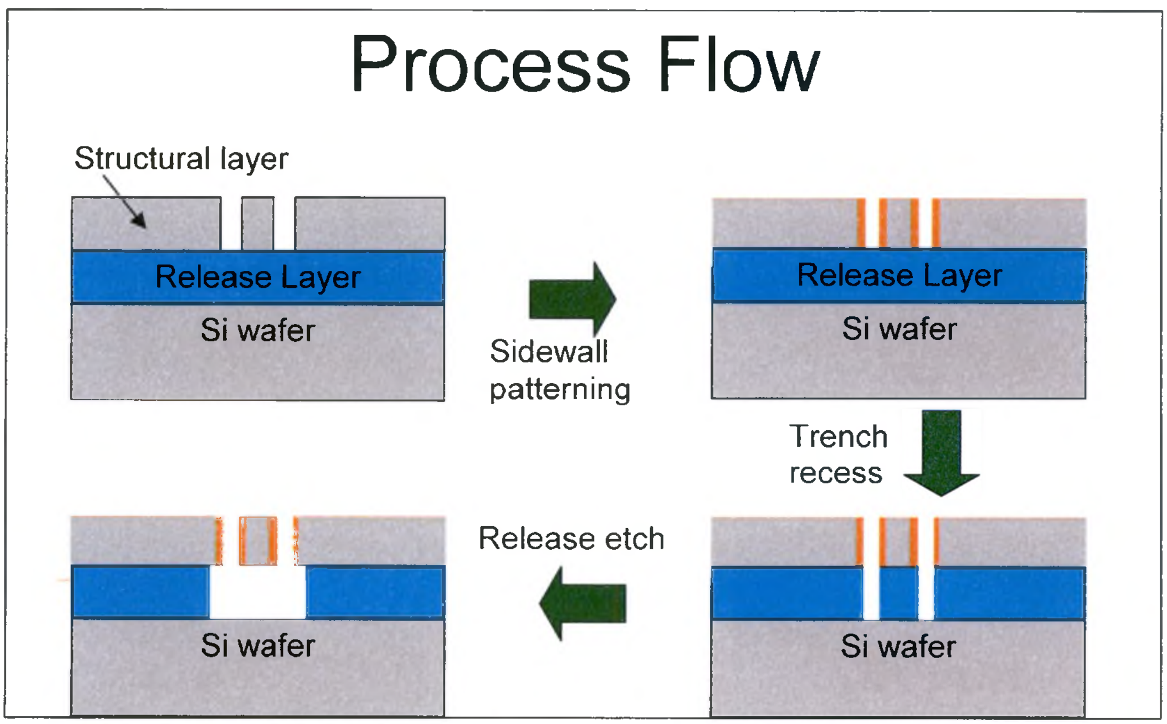

Fig. 2.1: Process flow for creation of NEMS cantilever.

Experimental Procedure

In order to test the NEMS cantilevers for their viability as a low power alternative to transistors, electrical and physical characterization data were collected, and simulations of the device expected performance were made. The electrical measurements were conducted with a four-point auto-probe at SEMATECH. The images of the tested devices were gathered using a JEOL 6400 FE scanning electron microscope (SEM) at Texas State University-San Marcos. Finally, the simulation of the cantilevers for various design parameters was conducted at Texas State using the COMSOL Multiphysics Simulation software.

Electrical Characterization-Background

A four-point probe has four probes each connected to a source measurement unit (SMU). Each of these SMUs can inject current, apply voltages, and measure voltages or currents at the same time. For the electrical tests done on the cantilevers each probe of the four-point probe was contacted with one of the four terminals of the cantilever devices. These contacts were then used to apply voltages and measure currents passing through the various parts of the device. The auto-probe then went through two tests for the contacted device. For the first test run, a voltage of 0. 1 V was applied to both the cantilever and driving electrode B. A voltage was then applied to driving electrode A and ramped from 0 V to 40 V (forward sweep) and then back down to 0 V (reverse sweep). While the voltage was ramped the current in all four terminals was measured with the compliance set to 1×10^{-7} A. The second test repeated this process with the two electrodes roles exchanged. So a voltage of 0. 1 V was applied to both the cantilever and driving electrode A. The voltage applied to driving electrode B was then ramped from 0 V to 40 V (forward sweep) and then back down to 0 V (reverse sweep). While the voltage was ramped the current in all four terminals was measured with a compliance set to 1×10^{-7} A. Once the auto-probe finished with these two tests it went on to the next device determined by preprogrammed vectors. This process continued until all of the devices on that die were tested, and then the auto-probe went on to the next die using another preprogrammed vector until all of the selected die on the wafer were tested. This process was used to collect data on all nine wafers and this data was provided by SEMATECH.

The data collected by the auto-probe from one of the two tests (either A or B being varied from 0 V to 40 V to 0 V) was then copied into Microsoft Excel with the software Metrics Miner. Once in Excel, a macro was run to sort the data into different categories. The first thing that the macro does when sorting out the data is to find devices that turned on. The macro does this by looking at the current in the active driving electrode at 40 V. If the current in the active driving electrode was above 9×10^{-8} A in macro, the device was considered to be turned-on. The reason that the macro checks the driving electrode current as well as the contact current is to check for device failure from the cantilever making unintentional contact with the driving electrode instead of the cantilever contact. Due to a design error, it was found that the cantilever makes a contact to the electrode the majority of the time instead of only coming into contact with the cantilever contact. The macro then searched for the voltage that the device first reaches compliance and sets that as the pull-in voltage. When the current in the active driving electrode dropped below a pull-out value (set to 1×10^{-8} A) and set that voltage was defined as the pull-out voltage. The macro then tested to see if the device turned on abruptly like a switch or if the device had a gradual turn on. The macro did this by checking to see if the current 1 V below pull-in voltage (V_{pi} - 1V) was smaller then a predefined gradual switch level (set to 1×10^{-9} A). If this current at the pull-in voltage minus 1 V was below the gradual switch level, the corresponding data with that device (the currents from the four terminals and the pull-in/pull-out voltages) was sent to an "electrode switch non-cantilever" category. This means that something (could be the cantilever or another terminal at this point) contacted the electrode and there was a fast turn-on in current for the device. If the current was above the switch level, the data from that device were sent to an "electrode non-switch non-cantilever" category. This means that there was a gradual turn-on of the current for the device, which could be caused by residue on the contact surface or by surface imperfections in the contact region.

To determine if the cantilever is operating properly, the macro does the same process as mentioned above, except the current from the cantilever contact terminal is measured instead of the current of the active driving electrode. Gradual switching was not tested for the cantilever contact terminal and any devices passing from this test are passed into a "contact to non-cantilever" category. This means that something came into contact with the cantilever contact. This could be the cantilever or could be another terminal at this point.

The macro then goes through these three categories and checks the current in the cantilever at 40 V. If the current at 40 V is above the compliance current the macro takes the associated data of that device and moves it into a corresponding cantilever category.

For instance, devices in category "electrode non-switch non-cantilever" would be moved to "electrode non-switch cantilever" if the cantilever contacted the driving electrode and turned on slowly. Devices in category "electrode switch non-cantilever" would be moved to "electrode switch cantilever" if the cantilever contacted the driving electrode and turned on quickly. Finally, devices in category "contact non-cantilever" would be moved to "contact cantilever" if the cantilever contacted the cantilever contact. From here the macro starts out by taking all the devices from these three categories that have a pull-in voltage below 2 V and placing them into the "short" category. The value of 2 V for the pull-in voltage was based on previous test data for this device, which showed that all devices with this low turn-on voltage had shorted. Finally, the macro goes through the "contact cantilever", "electrode non-switch cantilever", and "electrode switch cantilever" categories and checks the pull-out voltages to determine if any device has a higher pull-out voltage than pull-in voltage. Any device's that meet these criteria are placed into the "higher pull-out" category. The final test to check for passing devices is a visual inspection of the data to check for failures that the macro missed in the passing categories: "contact cantilever", "electrode non-switch cantilever" and "electrode switch cantilever". A flow chart of the folders that the macro uses to sort the data is seen in Fig. 2.2.

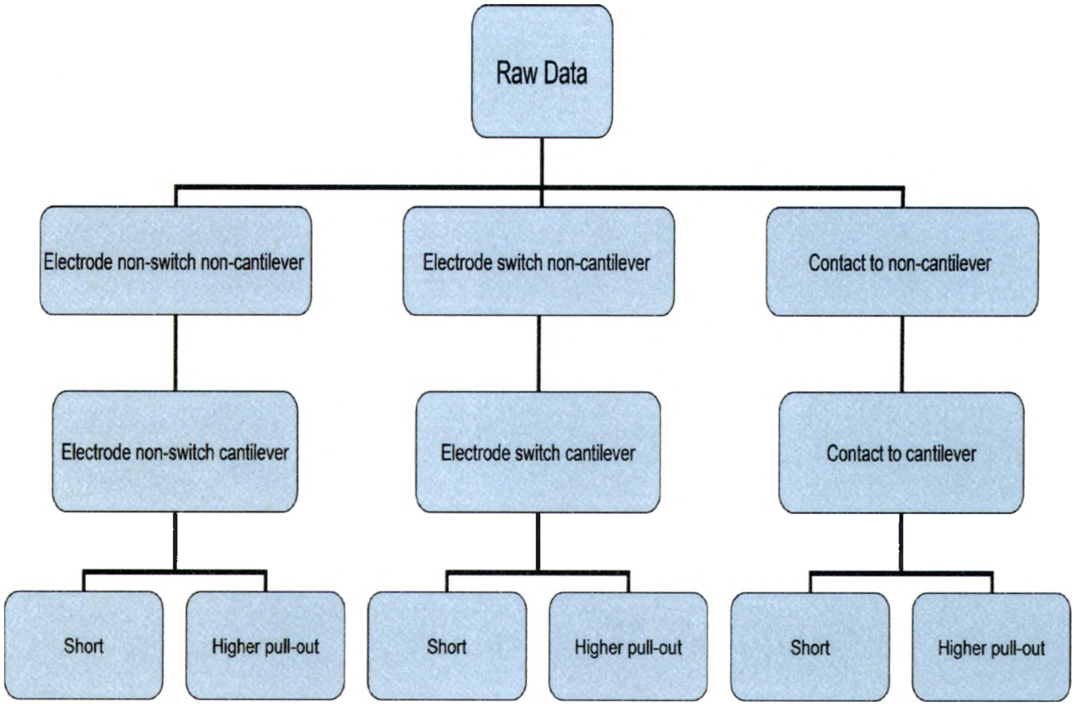

Fig. 2.2: Flow chart of macro bins.

Physical Characterization

A JEOL 6400 SEM was used to obtain the images. The SEM uses a beam of electrons to produce a highly magnified image of a sample. The image is produced from scanning the sample with a focused beam and detecting the secondary electrons that are emitted by the sample. The magnification from the SEM is dependent on the CRT size over the scan size. Generically an SEM consists of an electron source (that produces a beam of electrons), an electron lens system (focuses the electrons), scanning coils (moves the electron beam across the sample), an electron collector (that detects secondary electrons) and a cathode ray display tube (CRT) (that provides the topographical image). The SEM uses a beam of electrons to produce a magnified image of the sample.[11] This can be seen in the schematic below in Fig. 2.3, which was provided by Dr. Spencer.

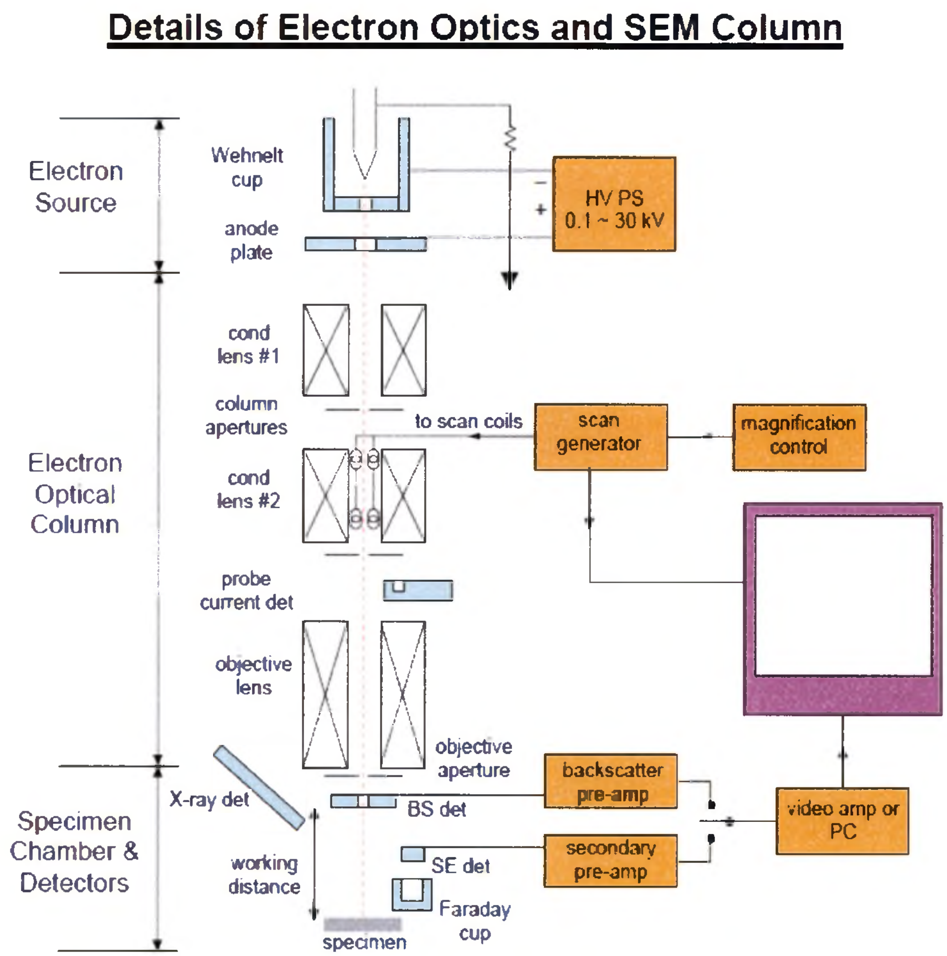

Fig. 2.3: Schematic of the JEOL SEM.

Since the wafers were too large to load into the SEM, they were cleaved into four quarters in order to insert them into the SEM. The wafer imaged for this study was wafer 6, which was selected because of the broad spectrum of passing and failing devices. The top left quarter was loaded onto the large sample holder. This was then inserted into the load lock and the lock was pumped down for insertion into the main chamber. A video camera inside the chamber was turned on to ensure proper placement of the sample onto the stage (working distance set to 15 and sample stage at HOME position). Once the load lock was pumped down the main chamber door was opened and the sample holder was placed onto the sample stage. The load lock was then closed and the main vacuum chamber began to pump back down to the operational pressures ($\leq 2\times10^{-6}$ Torr). The high tension voltage (10kV was used in these images) was turned on after the chamber pumped down and a 12 μA constant emission current was selected. A CL or spot size of the electron beam was varied between 6 and 7. Higher spot size numbers, corresponding to smaller spot sizes, create higher resolution on the sample from the decrease in spot size. The image of the sample was then focused and corrected for astigmatism at high magnifications while the scan size was kept small at 320 pixels. When the sample location and magnification were selected the scan size was set to 1240 pixels for a larger image. This was continued across all the devices tested on that particular die. Then it was continued on to the next selected die samples until all were imaged. The final step was to unload the sample and prepare the SEM for the next user. First the high tension was turned off and the magnification set to a value above 50k to reduce the strain on the scanning coils while the system is inactive. Next the sample stage was set to HOME to prepare to remove the sample holder. The load lock was then opened and the sample removed from the main vacuum chamber into the load lock. The load lock was then vented and the sample removed from the SEM. The next step was the pump down the load lock, turn off the camera and finally log off the computer.

Simulation

The COMSOL Multiphysics software package uses the finite element method (FEM) to perform its calculations. Within the software package three 3-dimensional modules were selected in order to do the simulation of the NEMS cantilevers. These include “Solid, Stress-Strain” which was used to model the material of the cantilever, “Moving Mesh (ALE)” which was used to update the mesh when the structure moved, and “Electrostatics” which was used to model the electronic fields and voltages. Once these three modules were selected, the structure was drawn with four boxes as can be seen in Fig. 2.4. The first box was designed to be the air gap and electrode face. The second box was designed to be the cantilever. The third box was designed to be the second air gap and electrode face. Finally the fourth box was designed to be the air surrounding the cantilever. See Table 2.1 for box dimensions. Now that the device has been drawn, the sub domains and domains of the various faces that these four boxes created are now ready to be inputted for the various modules.

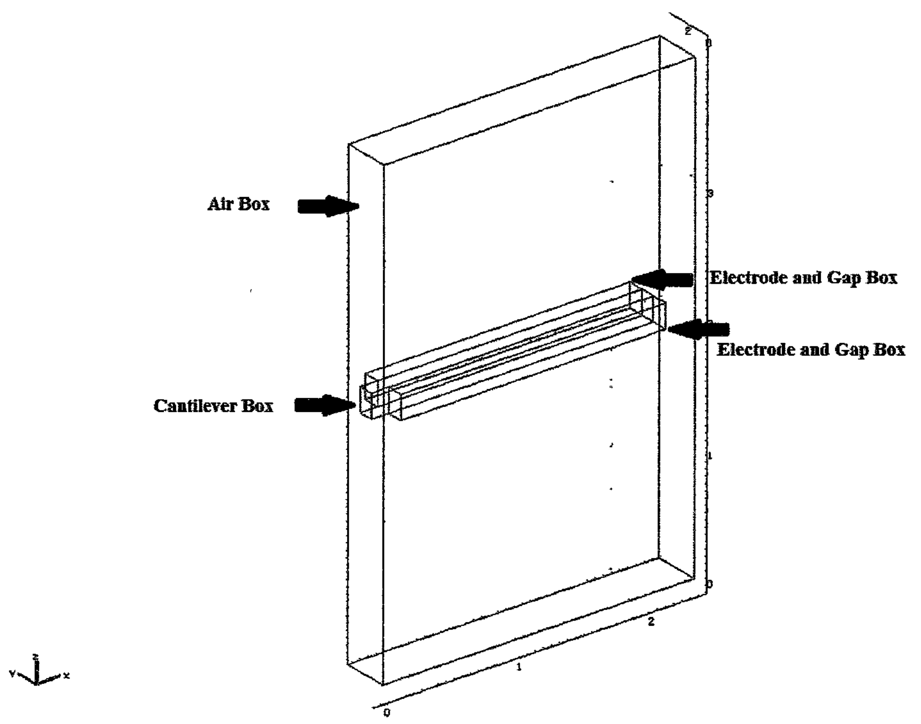

Fig. 2.4: Schematic of cantilever structure in COMSOL.

Table 2.1: NEMS cantilever Box dimensions for COMSOL.

CANTILEVER, AIR, GAP, AND ELECTRODE DIMENSIONS				
Axis base point	gap & electrode	Cantilever	gap & electrode	air
x	1. 3E-7 (m)	0 (m)	1. 3E-7 (m)	0 (m)
y	0 (m)	1. 2E-7 (m)	2. 3E-7 (m)	0 (m)
z	2E-6 (m)	2E-6 (m)	2E-6 (m)	0 (m)
Length	gap & electrode	cantilever	gap & electrode	air
x	2E-6 (m)	2. 13E-6 (m)	2E-6 (m)	2. 35E-6 (m)
y	1. 2E-7 (m)	1. 1E-7 (m)	1. 2E-7 (m)	3. 5E-7 (m)
z	2E-7 (m)	2E-7 (m)	2E-7 (m)	4E-6 (m)

In the "Solid, Stress-Strain" module, the cantilever (interior 2) is set to poly-Si under the sub domain option, while the rest of the options are unselected. Moving to the domains option for this module, the air and the body of the cantilever (faces 1, 2, 3, 4, 8, 9, 10, 11, 12, 13, 14, 16, 17, 18, 19, 20, 21, 22, 23, and 24) are set to free movement to allow them to move since the physics of the problem dictates that they move. The side of the cantilever that is facing the electrode (faces 6 and 15) is also set to free movement, but under the load tab the load is set to dnTx_enes for x, dnTy_enes for y and dnTz_enes for z, where dntx_enes, dnty_enes, and dntz_enes are functions being output by the electrical module. The bottom of the cantilever (face 7) is set to a symmetry plane to ease the problems calculations and increase speed of convergence. Finally the base of the cantilever (face 5) is set to "fixed" to provide the point where the cantilever would be connected to the probe pad and unable to move.

In the "Moving Mesh (ALE)" for the sub domain section the cantilever (interior 2) is set to "physics induced displacement" *u*, *v*, and *w* for *x*, *y* and *z*. The rest of the options were set to "free displacement". In the domain section the air (faces 1, 2, 3, 10, 12, 20, and 24) is set to zero displacement for dx, dy and dz. The base of the cantilever and the edges of the box from the air gap squares (faces 5, 11, 13, 14, 16, 18, 19, 21, and 23) are all unselected and the rest of the surfaces are set to u, v, and w for dx, dy and dz respectively.

In the "Electrostatics" module the cantilever (interior2) is set to poly-Si under the sub domain, and the rest of the selections were left as air. In the domain the cantilever (faces 6, 7, 8, 9, 15, 17, and 22) is set to 0.1 V and the air (faces 1, 2, 3, 4, 5, 10, and 24) is set to zero charge/symmetry. The air gaps edges (faces 11, 13, 14, 16, 18, 19, 21, and 23) were set to continuity, and finally electrode A and B (faces 12 and 20) were set to V_in1 and V_in2 respectively. Under the constants area, V_in2 was set to match the voltage applied to the cantilever.

A mesh was then initialized, and the parametric solver was then selected. Electrode A's voltage, V_in1, was varied from 0 to 40 V to determine the values of the pull-in voltage for various lengths (created by altering the 4 drawn squares). Direct Pardiso was selected as the linear solver with a tolerance of $1\text{x } 10^{-3}$ and 25 iterations. The linear solver was also selected to be Direct Pardiso, and a relative tolerance was set to 0.01, and an absolute tolerance was set to 0.001. The program was then run for the various parameter changes to size by altering the square sizes and material type by altering Young's Modulus under the "Solid, Stress-Strain" module in the sub domain cantilever (2). When the simulations were complete, the results were recorded in a domain plot parameter where the edge of the cantilever (19) had its *y*-displacement measured the applied voltage.

From a physics standpoint, COMSOL takes the parameters entered into the Solid-Stress Strain module and the four boxes drawn to create the cantilever structure. The simulation then takes the parameters entered into the Electrostatics module to place various charges and electric fields on the cantilever. Finally, COMSOL uses the Moving-Mesh (ALE) module to create a newly deformed cantilever structure as the voltage is ramped from 0 V to near the V_{pi} (the program stops converging at V_{pi}). This new deformed cantilever is then used for the next set of calculations determined by the electrostatics/solid-stress strain modules. In post processing, the V_{pi} can be obtained even though the data doesn't go all the way to V_{pi}, by extrapolating the curve to the y-intercept.

CHAPTER 3

RESULTS

Electrical Results

A random selection of 5 die across the nine wafers were tested in order to determine the relative pass rates for the wafers. This information was used to determine which wafers should be extensively tested. Out of all of the nominal gap/width (g_{elect}/w_{cant}) sizes, only the cantilever relays with nominal gap/width sizes of 110/100, 120/110, and 130/120 (where the sizes are given in nm) were tested to once again determine the highest yielding species. Once the gap/width size that produced the highest yield was determined, this subset was extensively tested across a large portion of the die on a wafer to obtain meaningful statistics for the pull-in voltages. The results of this test are shown in Table 3.1. From this table wafer 4, 5, and 6, which all have a 600 nm sacrificial oxide layer, were determined to have the highest yields. This suggests that the anhydrous vapor etch is playing a role in the failure of the devices since the success rate is much higher for a sacrificial layer of 600nm vs. 800 nm and 400 nm. The variation of sacrificial layer thickness was done to determine the optimal pocket size for the cantilevers, which prevents contact with the substrate because of drooping. If cantilever drooping was the only cause for device failure, the largest sacrificial layer size should have the highest pass rate, which was not the case.

Table 3.1: Yield rates for the nine wafers.

RELATIVE PASS RATES FOR WAFERS									
wafer	1	2	3	4	5	6	7	8	9
g_{elect}	Passes								
110nm	8	3	3	1	4	4	4	3	6
120nm	3	0	2	10	6	10	0	0	1
130nm	2	0	3	6	6	4	1	0	1
Total	13	3	8	17	16	18	5	3	8

Electrical data were taken from wafers 4, 5, and 6, which each have a different doping density of the poly-Si, but all with a sacrificial layer of 600 nm. A g_{elect} of 120 nm and a w_{cant} of 110 nm were selected due to its high yield ratio. All of the cantilever lengths (l_{cant}), 2 μm up to 14 μm were tested across the entire wafer. The pull-in and pull-out voltages for devices that contacted the driving electrode were then placed in a scatter plot for various device lengths and graphed for electrode A and for electrode B as seen in Figs. 3.1-3.3. From the large variance in the pull-in voltages across all of the wafers, the effect that the doping density has on the pull-in voltage can not be determined with the current data. However, a general trend for the wafers is that the pull-in voltage at l_{cant} = 2 μm starts at about 25-30 V and then evens out at about 10-20 V for l_{cant} = 4-14 μm. This result does not agree with equation 9, which predicts that the displacement of the cantilever should increase linearly with length of cantilever for a given applied voltage. This might be due to bending of the cantilever at a location other than the base, or may be from drooping of the cantilever in the z direction, which would cause an increase in the pull-in voltages for the larger device lengths. Another cause of the large variation in pull-in voltages could be the cantilevers not fully releasing during processing, but breaks free during the test increasing the pull-in voltage. No general trends from the wafers can be inferred from the electrode B sweep data due to the large number of failures created by the electrode A sweep. This increased failure rate becomes especially evident for wafer 5 where l_{cant}= 2, 4, and 8 μm did not have a single working device after the electrode A sweep. If electrode B had been swept first, it is assumed that some of the devices would have actuated properly.

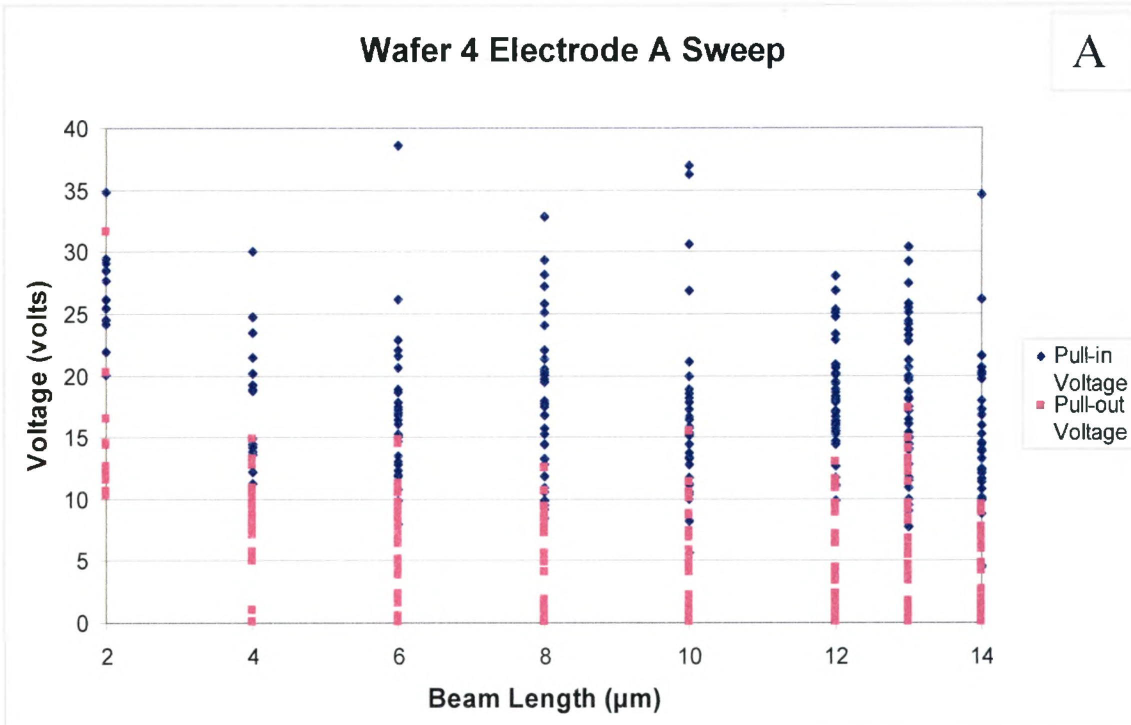

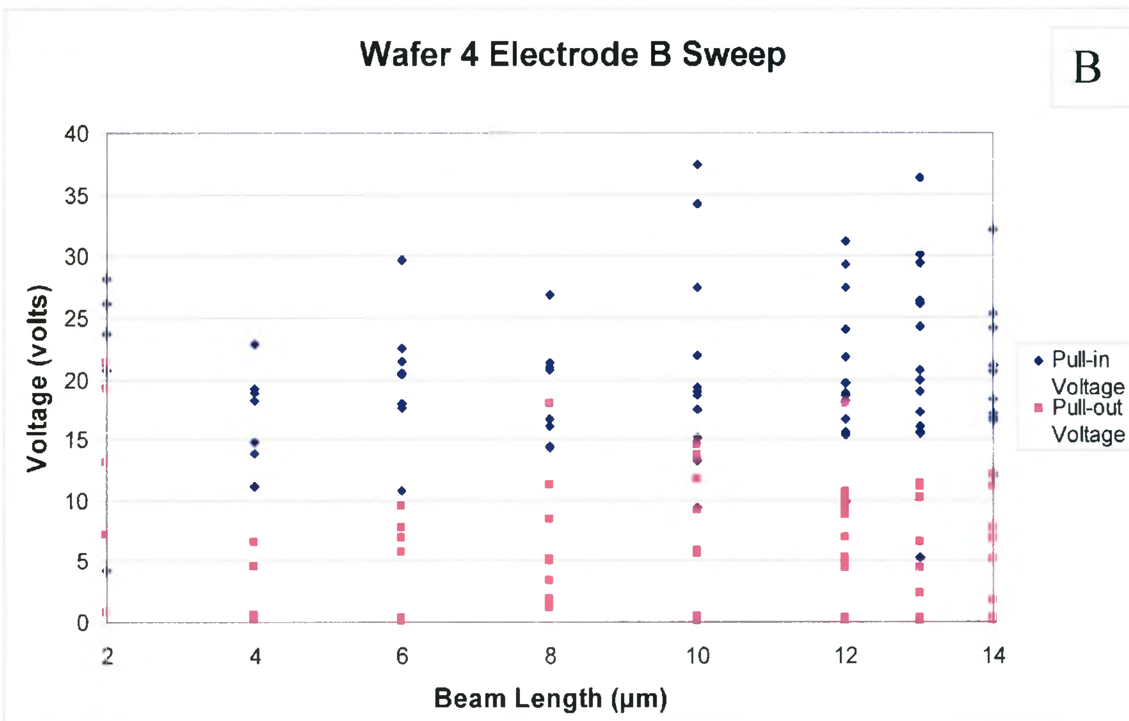

Fig. 3.1: Pull-in/Pull-out voltages for A and B electrode sweeps for wafer 4.

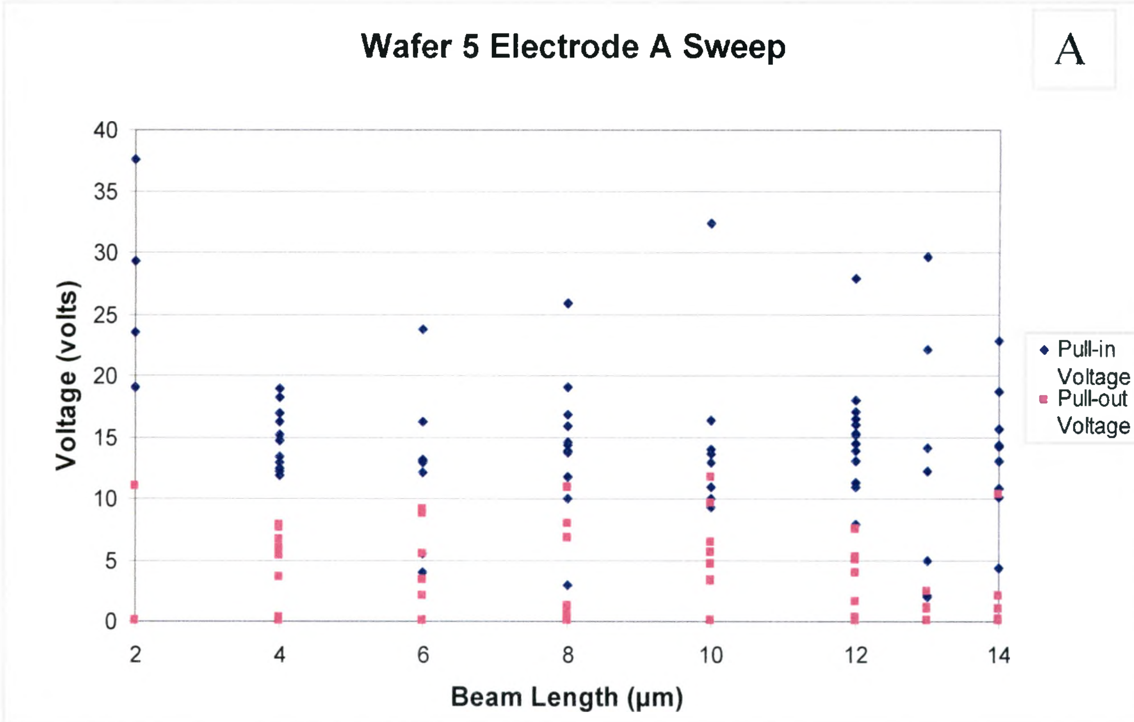

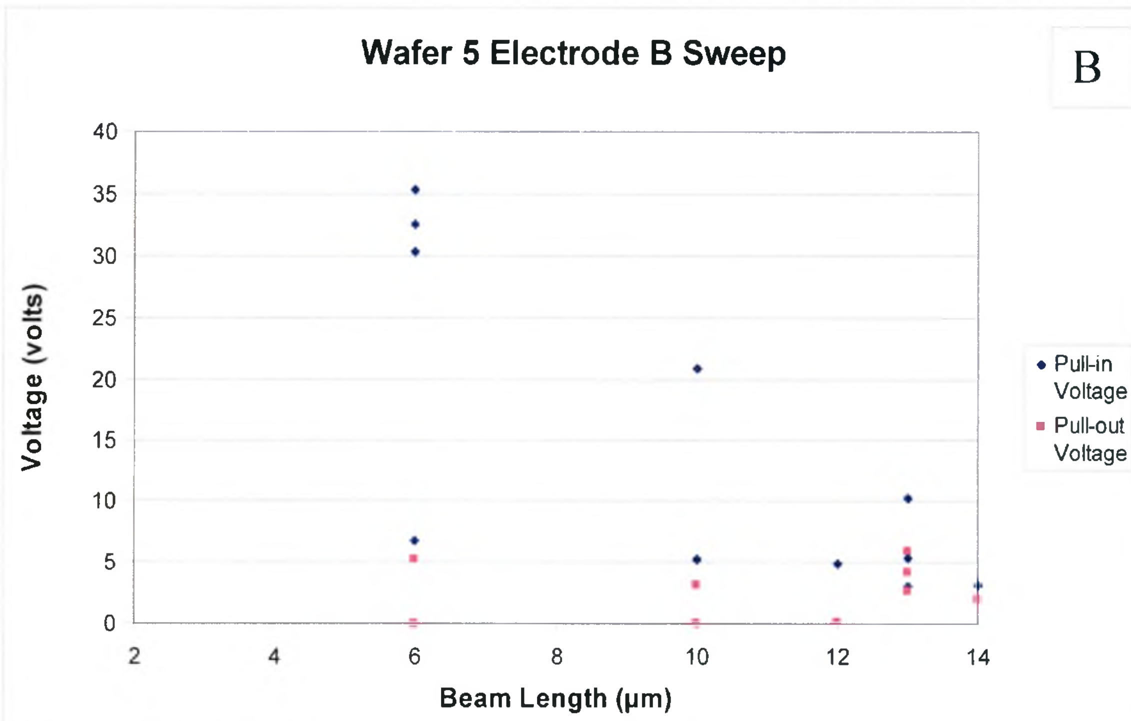

Fig. 3.2: Pull-in/Pull-out voltages for A and B electrode sweeps for wafer 5.

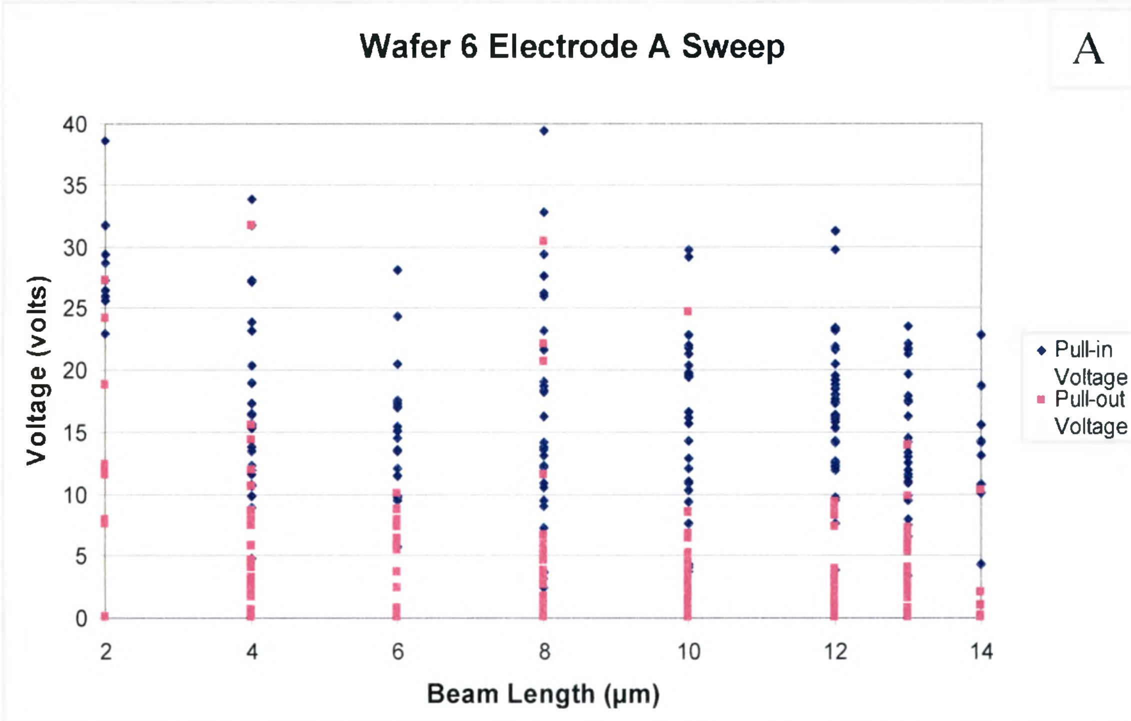

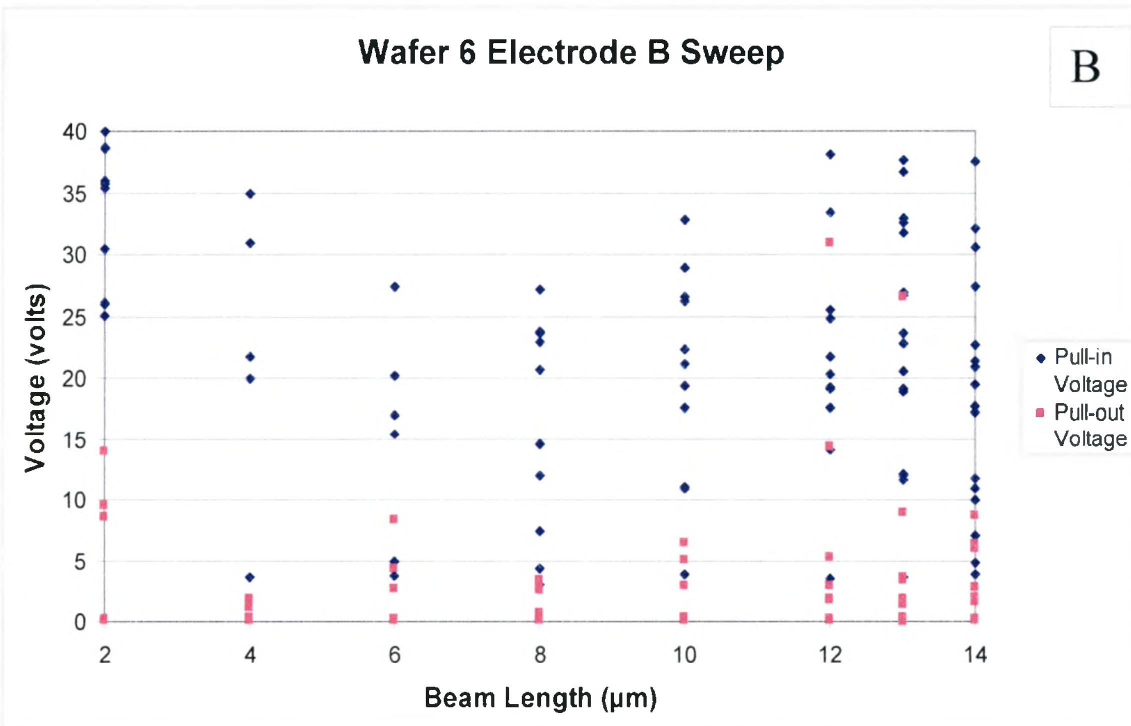

Fig. 3.3: Pull-in/Pull-out voltages for A and B electrode sweeps for wafer 6.

A map of wafer six for device length 12 μm(l_{cant}=12) is shown in Fig. 3.4. This information is used to get an idea of where the devices were passing as well as if the device worked for both the Electrode A and B sweep (Fig. 3.3). In the wafer map the numbers represent the coordinate system where the top half of the die is the x coordinate and the bottom half is the y coordinate. It should also be noted that die (0, -10) had been previously tested. This means the device is switching for the second time and demonstrates the NEMS cantilever switch concept.

For each die on the wafer map, the top half of the die box, represents the electrical data from the Electrode A sweep. If the top half of the box is colored green it means that the device passed and the pull-in voltage is under one standard deviation from the average of the pull-in voltage for that cantilever length. If the color is yellow the device still is a pass but the pull-in voltage is greater then one standard deviation. Finally if the color is red it represents a failed device. The bottom half of the die on the map represents the electrical data from the Electrode B sweep. If this half is blue it means that the device is a pass and the pull-in voltage is under one standard deviation, if the color is purple the device is still a pass but the pull-in voltage is greater then one standard deviation, and if the color is orange it represents a failed device. See Fig. 3.4 for a legend. It can also been seen from the map that a fail in Electrode A sweep does not mean a failure of the Electrode B sweep. Because most of the Electrode B sweeps failed after an Electrode A sweep, the failure mechanism is believed to be caused from the cantilever fusing to the driving electrode. This is further investigated in the physical characterization section

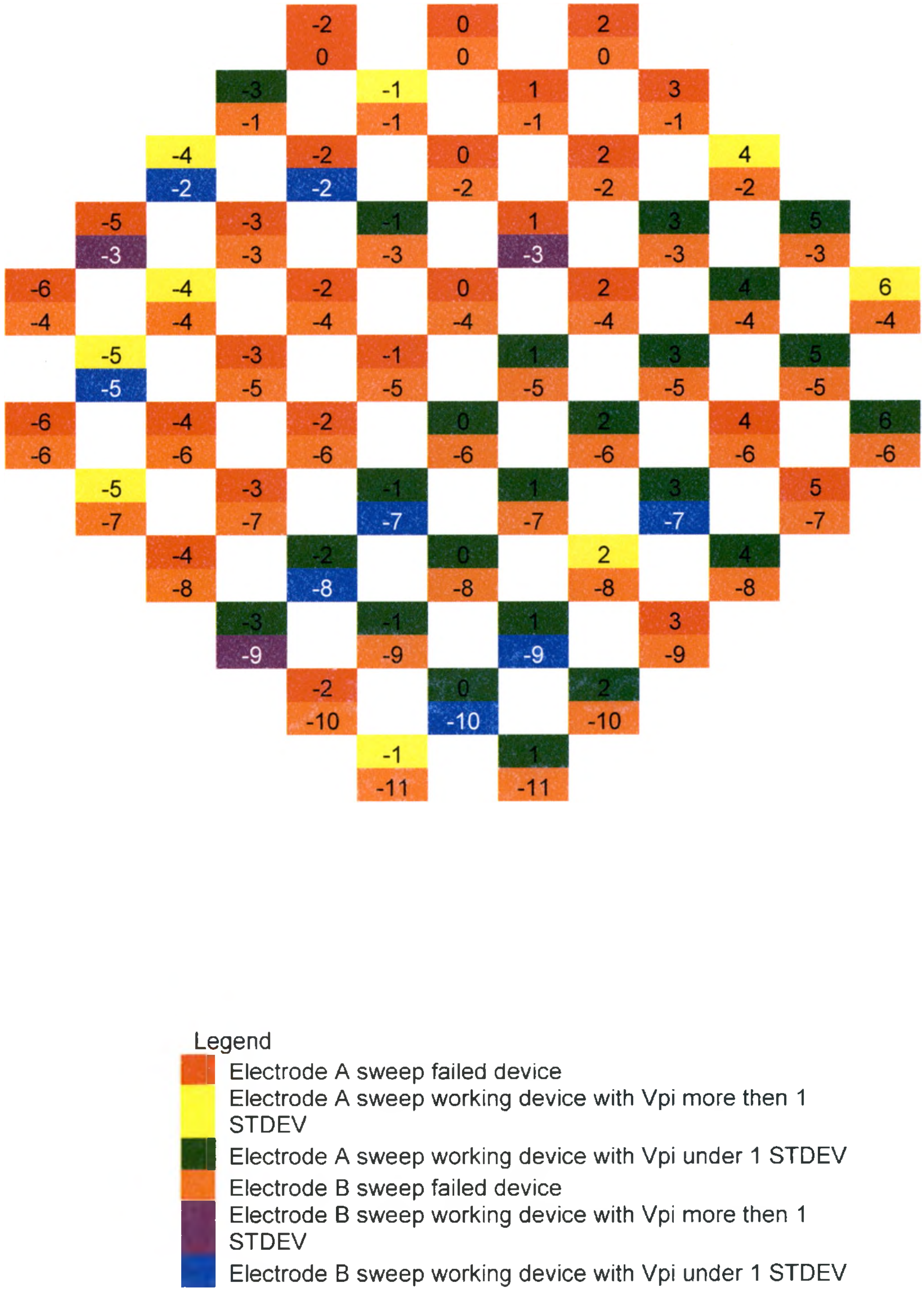

Fig. 3.4: Wafer map for wafer 6, cantilever beam length 12 μm.

Physical Characterization Results

Various devices of length l_{cant} = 2-14 μm, width w_{cant} = 110 nm and electrode gap g_{elect} = 120 nm were selected from wafer six and were imaged by SEM. These images were taken after the two electrical tests. This allowed for a comparison of the device conditions with the electrical data corresponding to the last test done, the Electrode B sweep. This information was then used to determine the mode of failure of the devices that did not switch properly.

Since there were a large number of device failures, it is assumed that there is a design flaw in the cantilever. In particular, the design is particularly prone to unintended electrical contacting of the cantilever with the driving electrode before contact with the desired cantilever contact. It is assumed that the shorting to the electrode results from receding or increasing in the size of the contact gap during processing. For instance, it can be seen in Fig. 3.5 that the electrode gap is smaller in some places than the cantilever contact gap. In addition, excessive vertical drooping can also cause the cantilever to never make contact with the cantilever contact. As seen in Fig. 3.6, the cantilever is seen to be drooping at the cantilever contact side, but not at the base of the cantilever. This is for a cantilever of length l_{cant}= 2 μm. For longer devices this effect would be even more pronounced and could be another possible reason for why the cantilever sometimes failed to make contact with the cantilever contact.

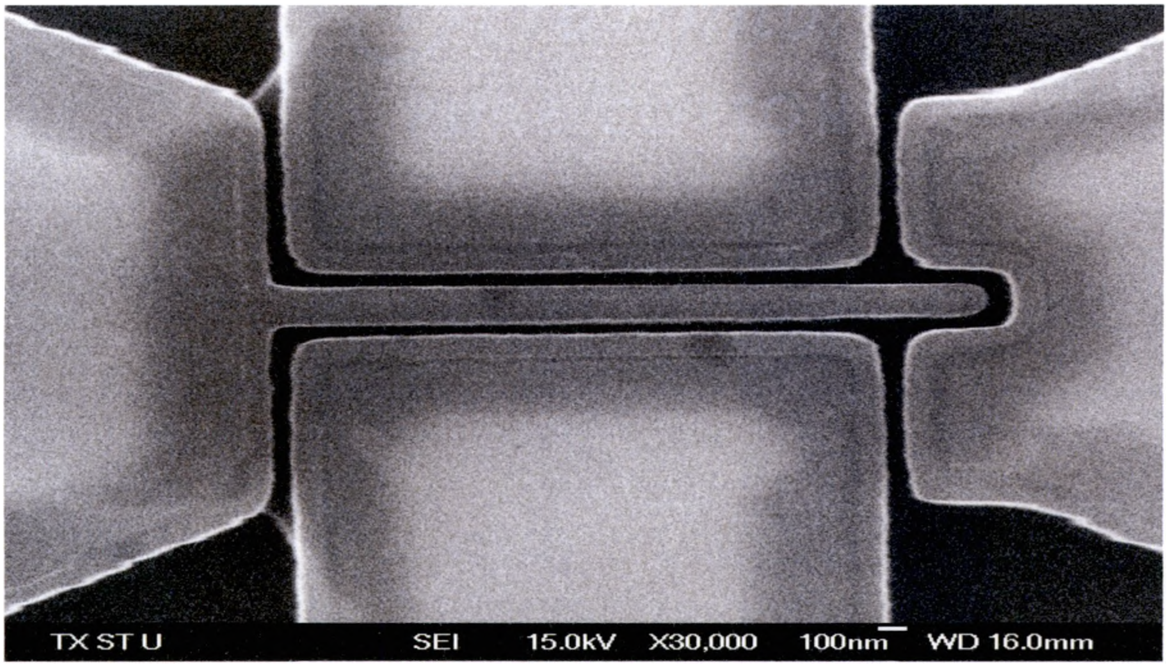

Fig. 3.5: Wafer 6, cantilever beam length 2 μm, die (-4,-1), shows the smaller electrode gap than the cantilever contact gap.

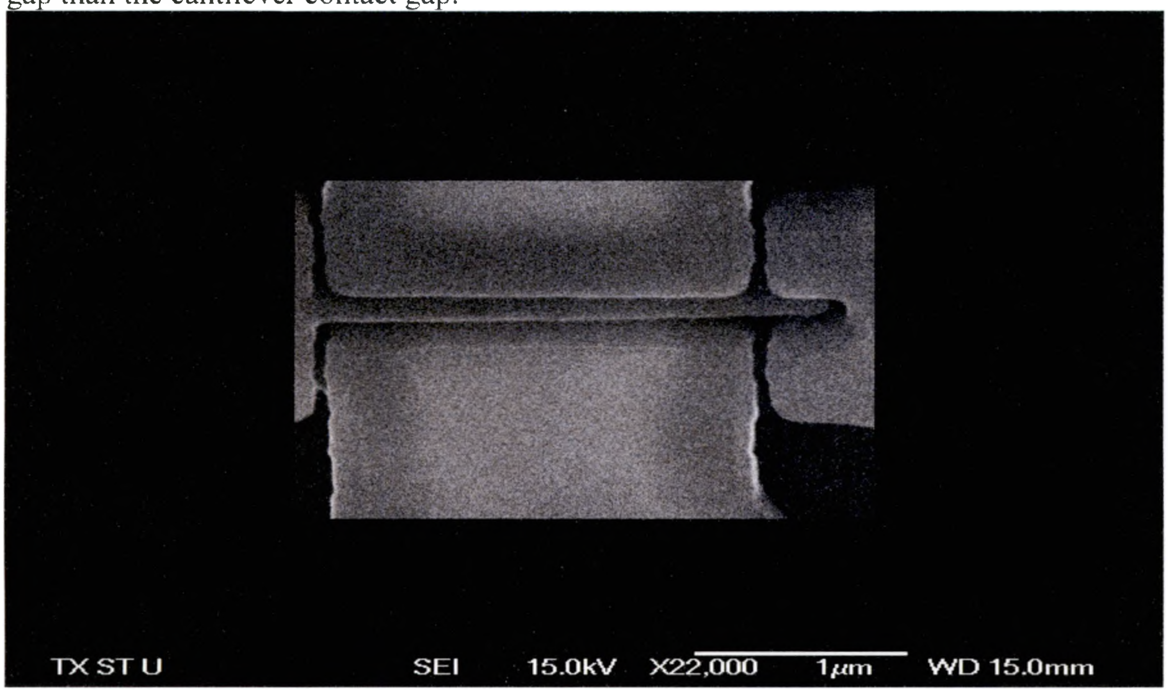

Fig. 3.6: Wafer 6, cantilever beam length 2 μm, die (-4,-1) at 45 degree tilt, shows the cantilever drooping near the cantilever contact.

Cantilever Contact Loss Devices

Some of the cantilevers come into contact with both the cantilever contact and the driving electrode at the same time during the pull-in stage of the electrical test. For most of these events, the contact to the cantilever contact is broken shortly after connection, while the contact to the driving electrode remains (see Fig. 3.7a). There are a couple of possible mechanisms for this to happen. For instance, the tip of the cantilever could fracture or bend after the cantilever contacts the driving electrode. It is also possible that the contact area at the end of the cantilever may degrade, resulting in the formation of an insulating SiO_2 barrier that prevents conduction into the cantilever contact. An example of a cantilever that failed with this mode is shown in Fig. 3.7b. As can be seen in the SEM image, the cantilever is bent and appears to be connected to both the driving electrode and the cantilever contact. Since the electrical current to the cantilever contact went to zero, there must be an insulating barrier at the connection point to the cantilever contact.

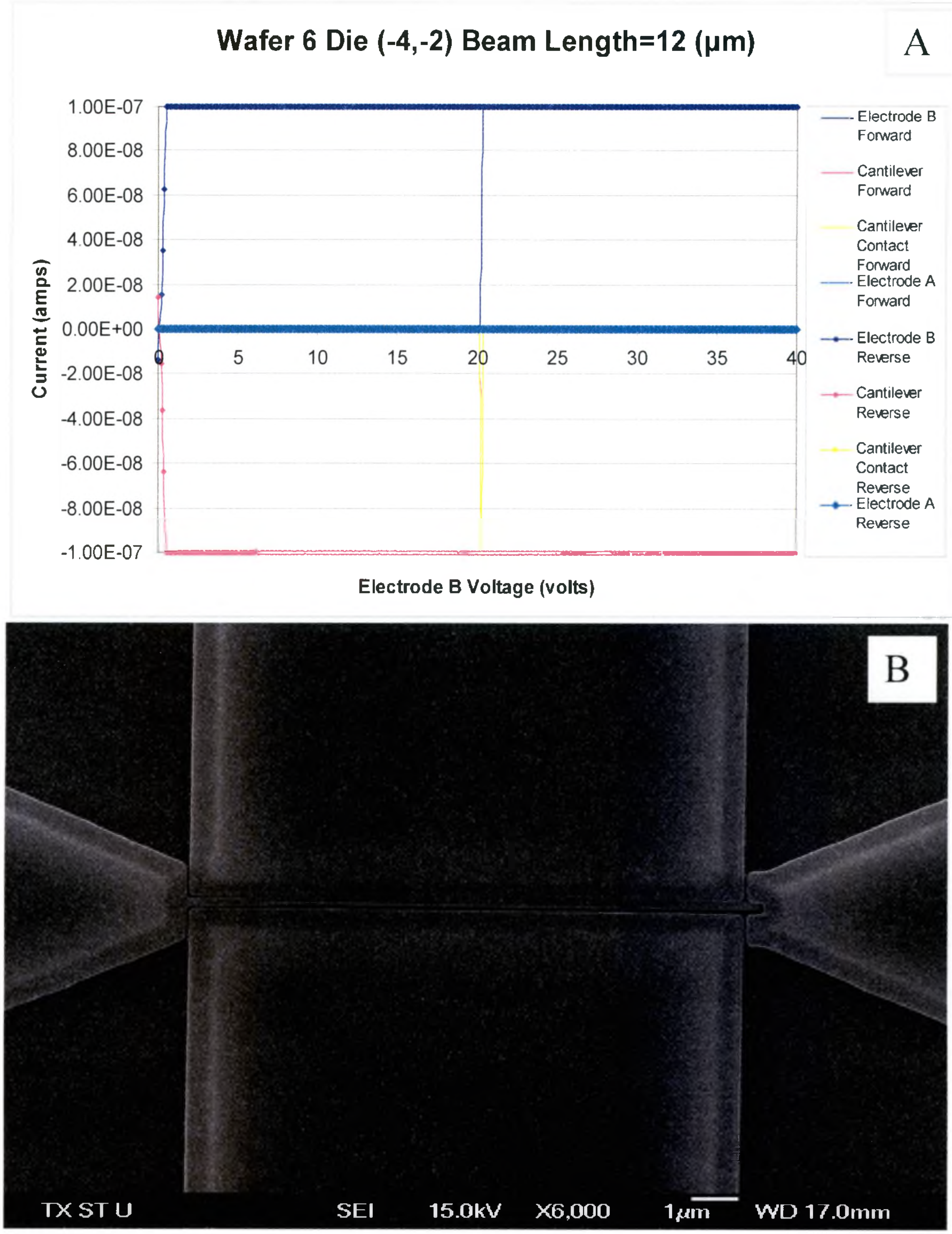

Fig. 3.7: Device displaying a loss of contact to the cantilever contact during connection.

Higher Pull-out Devices

Some of the cantilevers had a higher pull-out value than the pull-in value as seen in Fig. 3.8a. From Eqn. 9, the forces involved in actuating the cantilever should become greater as the distance decreases. This means that when the cantilever and electrode snap together during the pull-in stage, it should take less voltage to hold the cantilever in place. The short-range Van der Waals interaction that exists when two surfaces meet also plays a role in holding the two terminals together. This would further reduce the voltage required to hold the cantilever in place. The reason for these anomalies is unclear from the electrical data. The SEM image shown in Fig. 3.8b does not reveal an obvious cause of this effect. Since the cantilever seems to be in contact with the driving electrode and the cantilever contact, it is expected that there should be both a driving electrode current and a cantilever contact current as the driving electrode is ramped below the pull-in voltage, but this was not observed.

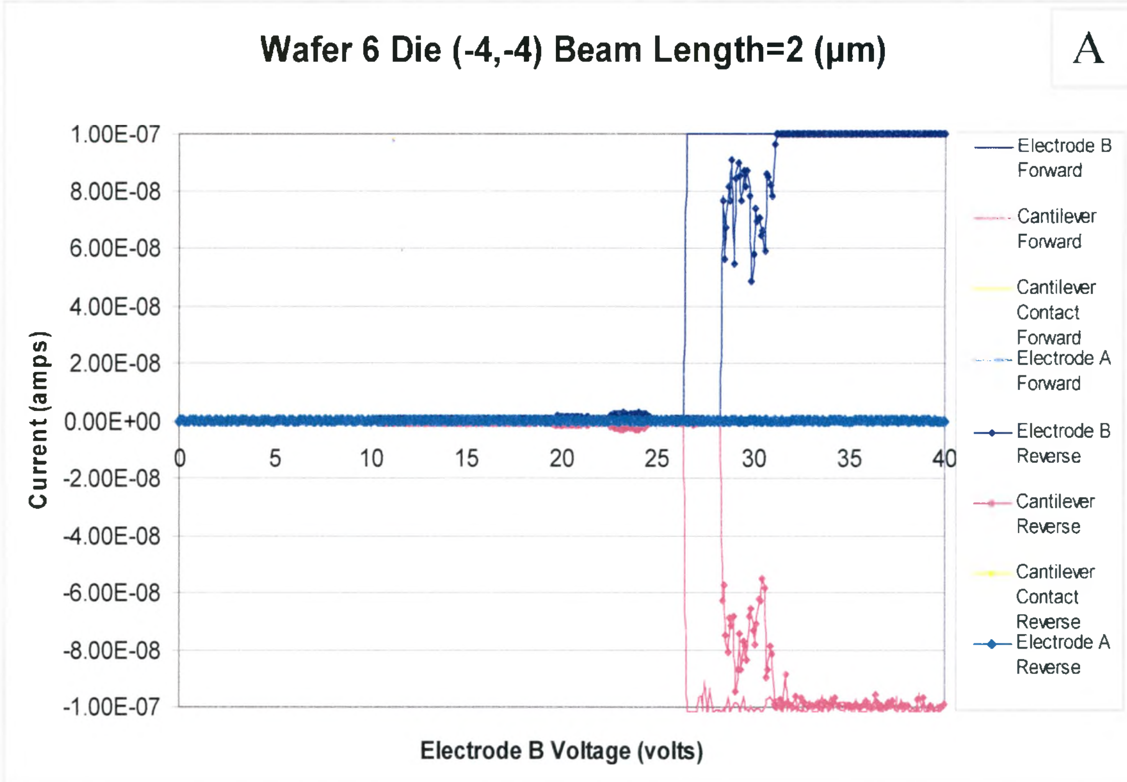

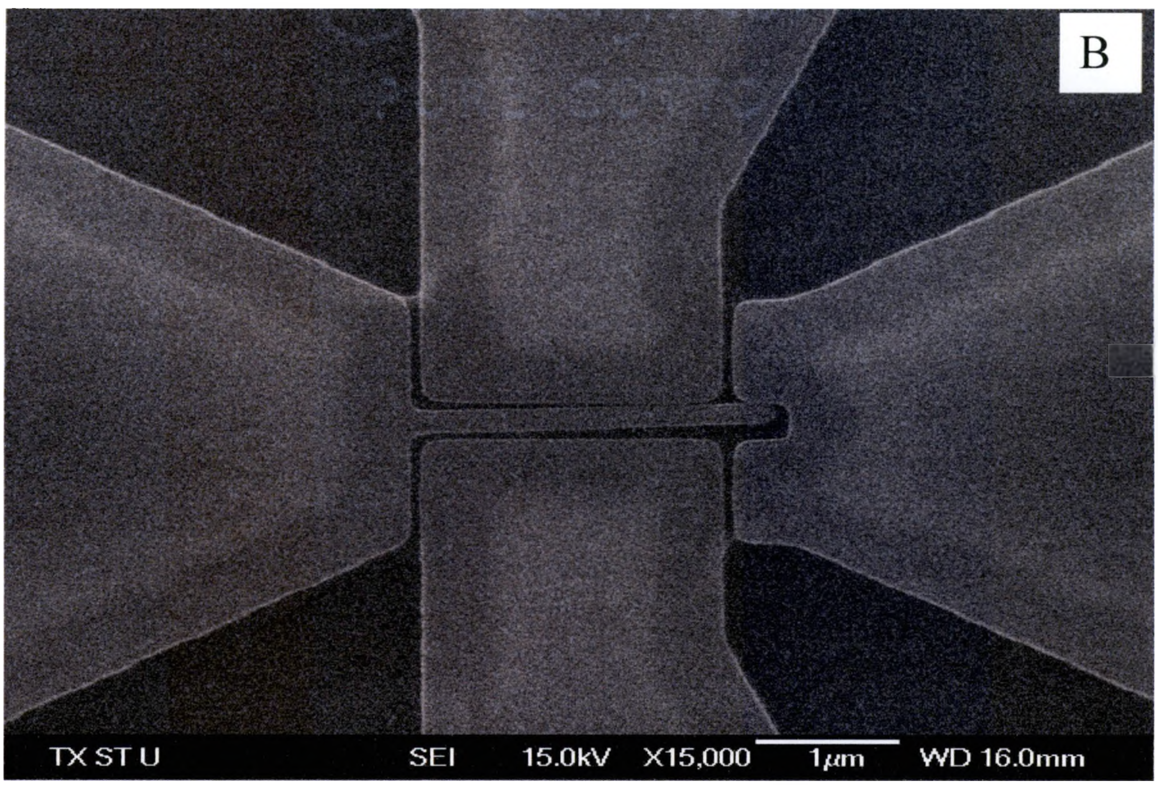

Fig. 3.8: Device displaying a higher pull-out than pull-in voltage.

Shorted Devices

Some of the cantilevers were shorted devices. Based on previous experience with these cantilevers, any device that actuated below 2 V was automatically categorized as a shorted device. For instance, the current curves for a shorted device are shown in Fig. 3.9a. For this device, driving electrode B is shorted starting at 0V bias. As seen in Fig. 3.9b, the cantilever appears to make contact with electrode B and the cantilever contact. However, the electrical data indicate that there is no contact to the cantilever contact.

An example of a device with all four terminals shorted together is shown in Fig. 3.10. From Fig. 3.10a, it can be clearly seen that at the start of the electrode A sweep there was a short between electrode B and the cantilever. This device was probably shorted to electrode B sometime during processing. In the electrode A sweep, the cantilever was pulled into electrode A at about 39 V and became fused creating a device that was fused to all terminals. This is shown by the electrical data (Fig. 3.10a and Fig. 3.10b) and in the SEM image shown in Fig. 3.10c.

This same phenomenon can be seen in Fig. 3.11. During the electrode A sweep the cantilever became fused to electrode A when the two connected as can be seen in Fig. 3.11a. After the electrode A sweep the electrode B sweep was run. The bridged structure, this time caused by the electrode A sweep instead of processing, connected with the electrode B terminal and became fused as can be seen in Fig 3.11b. The SEM image of the device (Fig. 3.11c) shows that the cantilever is connected to all of the terminals as is indicated by the electrical data.

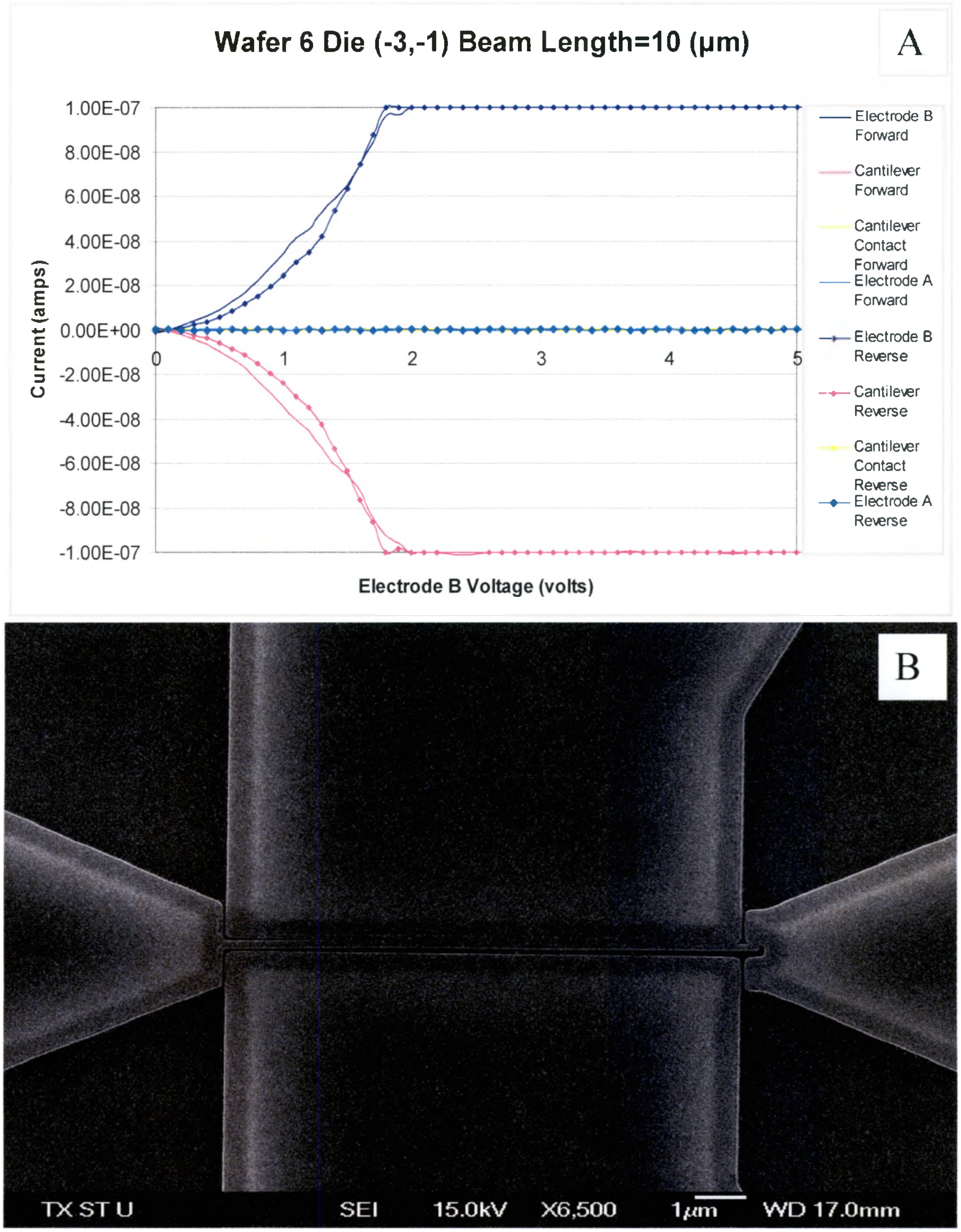

Fig. 3.9: A shorted device with pull-in under 2 V.

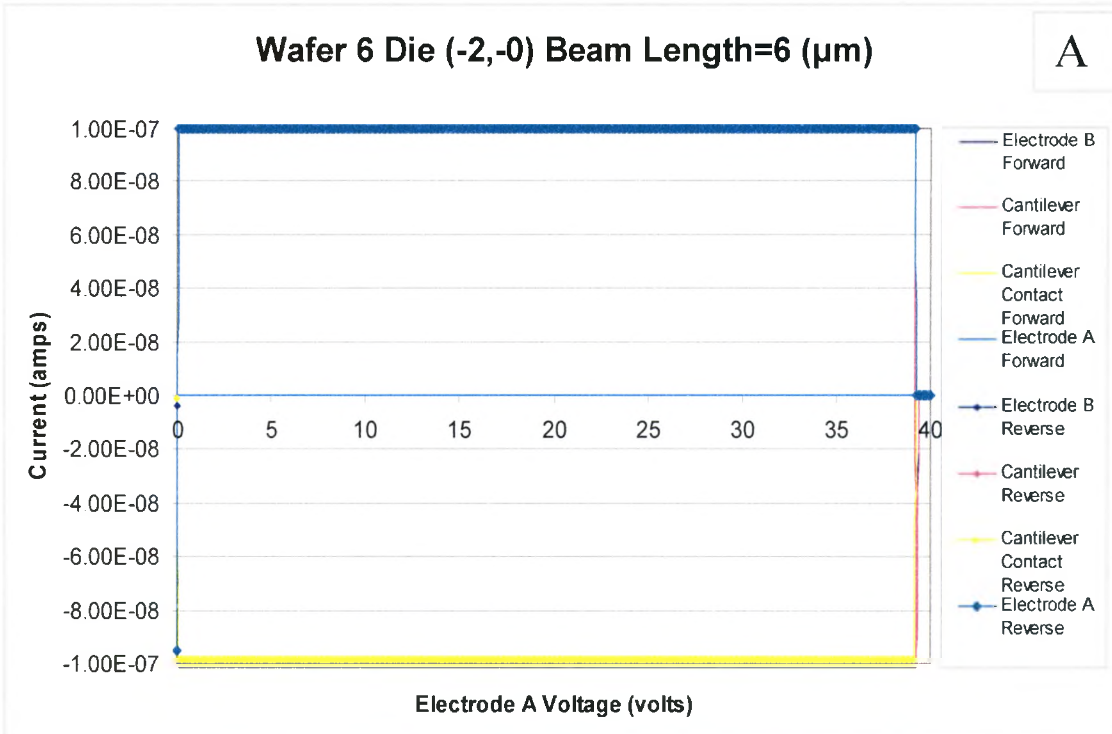

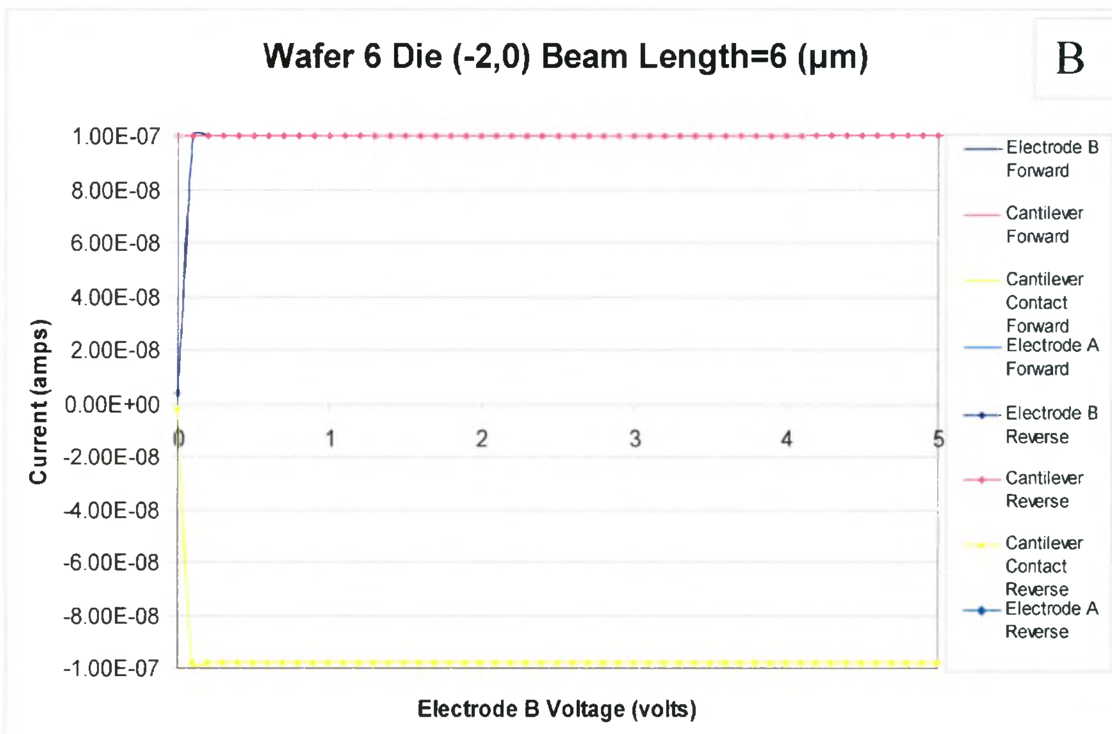

Fig. 3.10: Device with a short between electrode B and cantilever sometime during processing that shorted to all terminals during electrode A sweep.

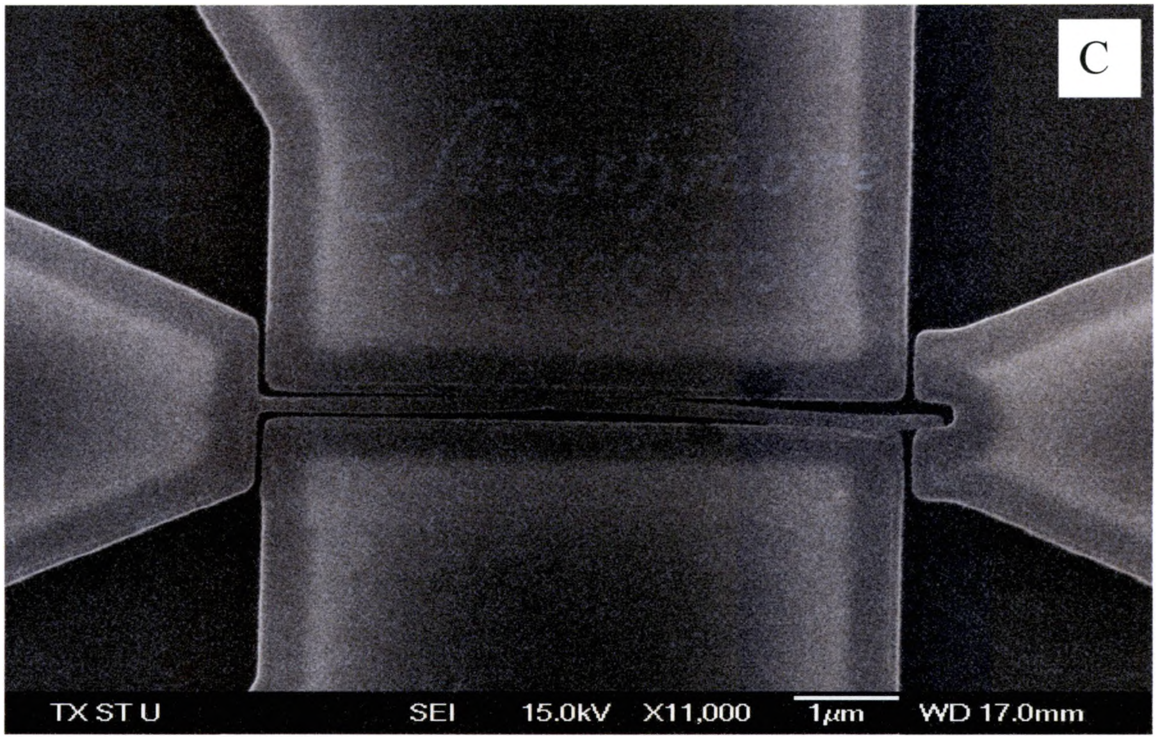

Fig. 3.10: Continued.

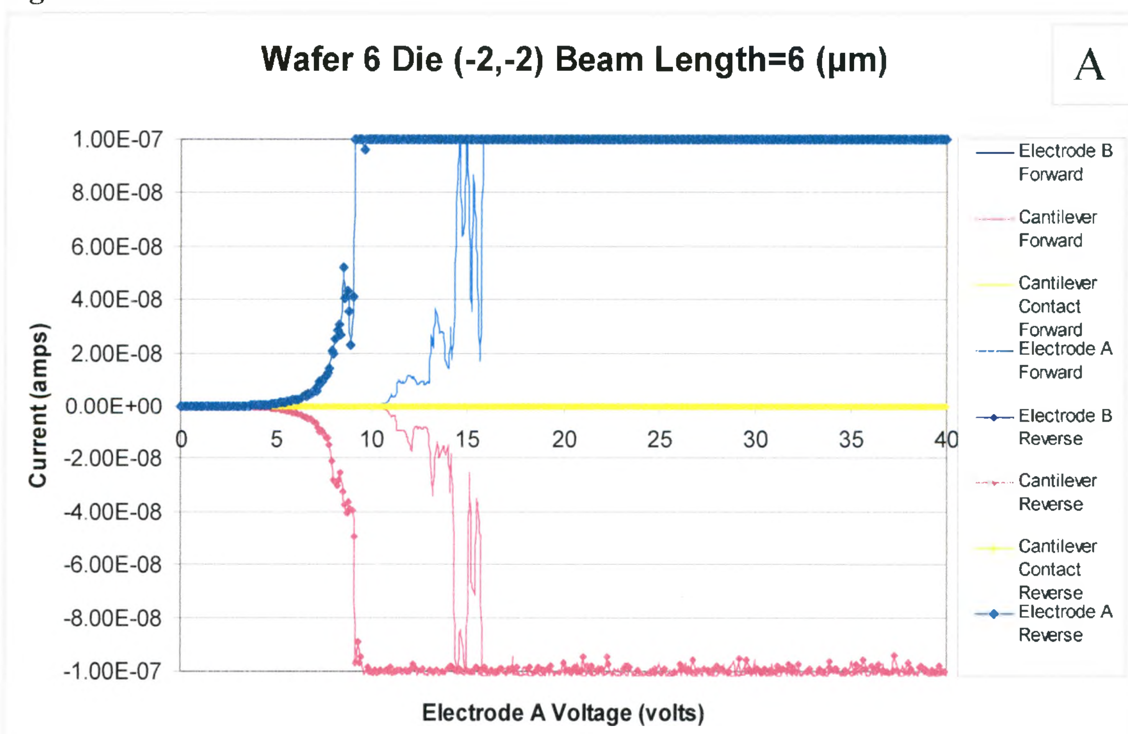

Fig. 3.11: Device that shorted between electrode A and the cantilever during the electrode A sweep and then shorted to the rest of the terminals during the electrode B sweep.

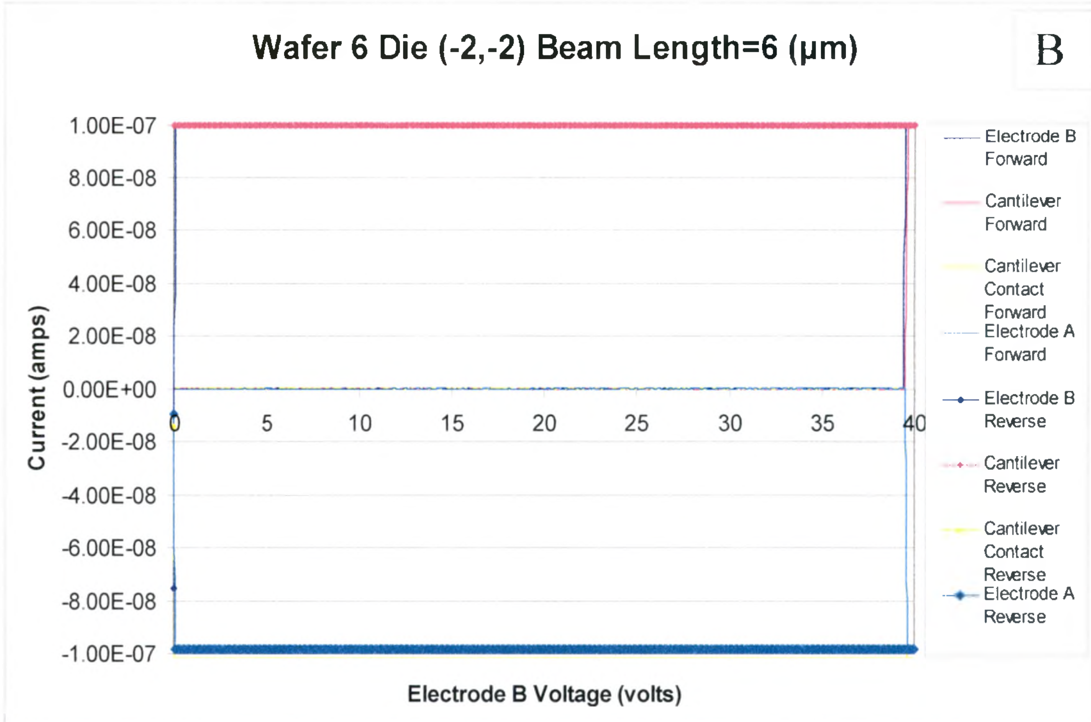

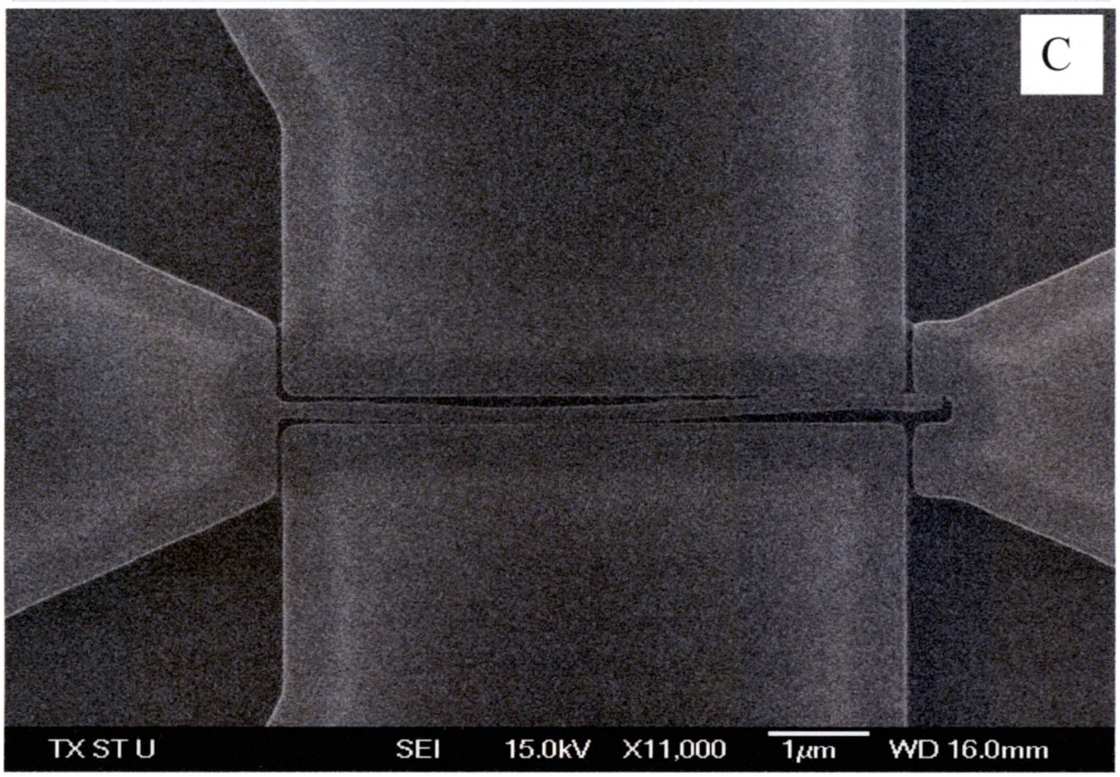

Fig. 3.11: Continued.

No Actuation Devices

In some cases, the failure mechanism was not obvious from the electrical data. For instance the electrical data for the device shown in Fig. 3.12a shows no actuation. However, it is clear from the SEM image shown in Fig 3.12b that the cantilever is fractured in several places. Therefore, the cantilever is probably too fractured to allow electrical current to flow through it, even though there is a physical connection between the cantilever and all of the terminals.

Another example of a device that did not actuate during the electrode B sweep is shown in Fig. 3.13a. From the SEM image (Fig 3.13b), there can be seen a slight tilt of the cantilever with respect to the driving electrode. Other than the observed tilt, the device appears to be normal. This failure may have been caused by the cantilever not fully releasing during processing, which would prevent the cantilever from actuating during the tests.

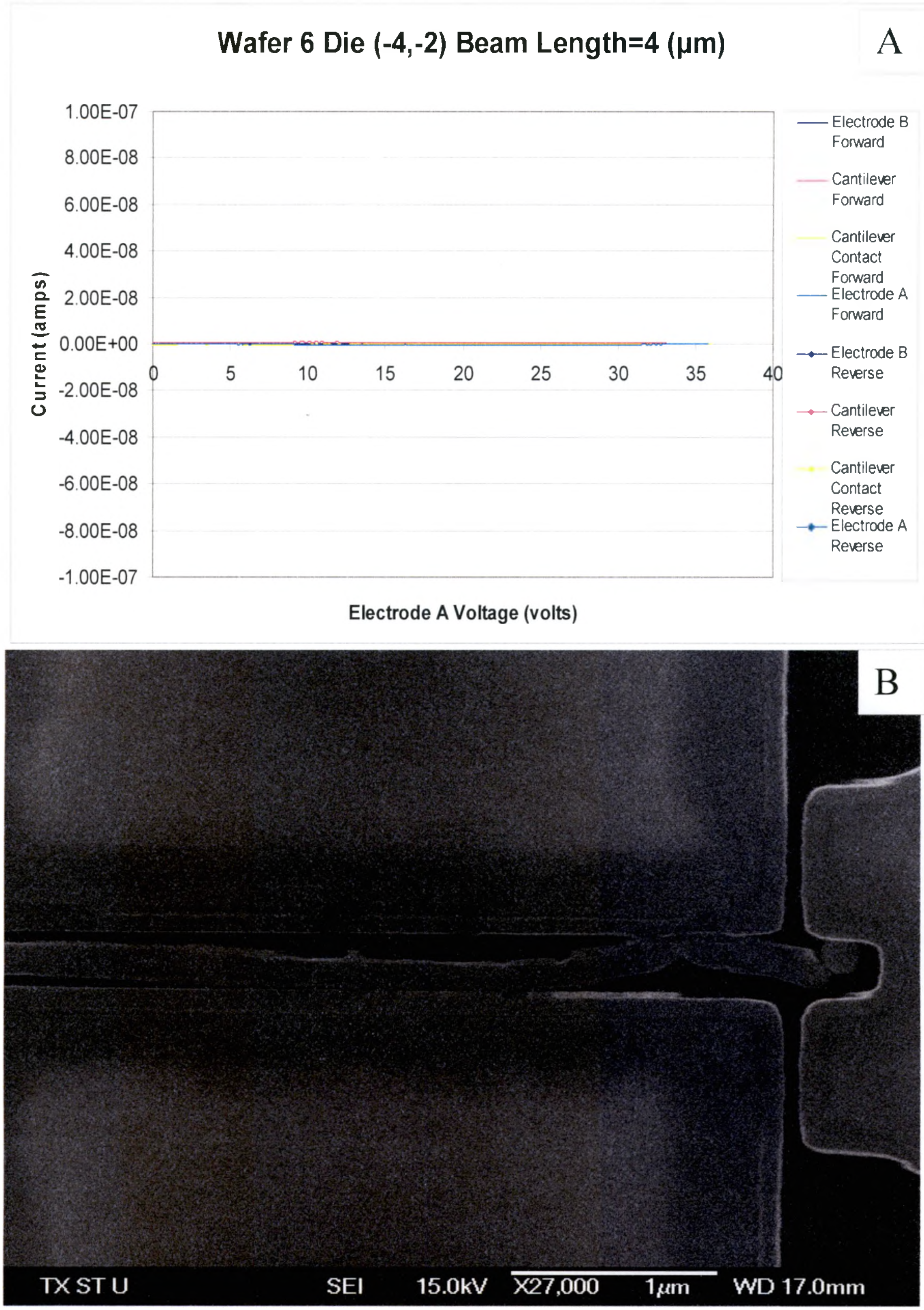

Fig. 3.12: Device that did not actuate and shows fractured cantilever beam.

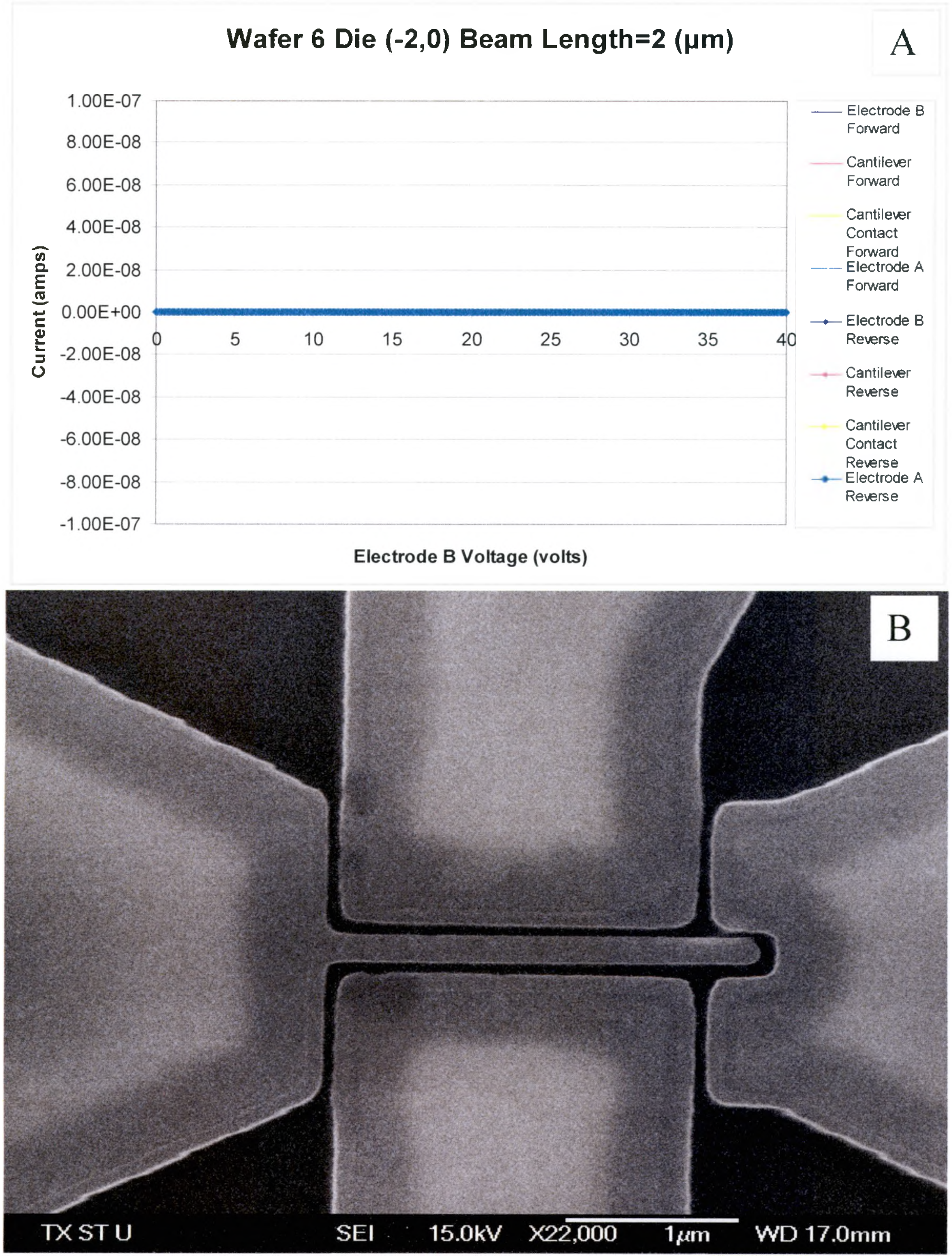

Fig. 3.13: Device that did not actuate and seems normal from SEM.

Fused Devices

Finally, there are the cantilevers that switched on, but became fused when they came into contact with the driving electrode. This is a leading cause of failure for the devices. The reason for the fusion upon contact with the driving electrode is the large current induced by the high voltage on the driving electrode. The device was not designed to come into contact with a terminal with high voltage, but was designed to contact the cantilever contact, which does not have a high voltage applied to it.

An example of a switching device that got shorted when it switched on is shown in Fig. 3.14. Another example of a switching device that shorted when it turned on is shown in Fig. 3.15. However, for this device the fused area is at the end of the driving electrode, near the cantilever contact. This created a fused pull-out that has a gradual turn-off. An example of a device that had current before it pulled in is shown in Fig. 3.16. This is probably from residue from the etch coming into contact with one of the terminals. It can also be seen in Fig. 3.16a that there is a very small connection to the electrode A for this device. In the SEM image (Fig. 3.16b), it can easily be seen that there was a poor etch of this device. This device also fused together when it turned on.

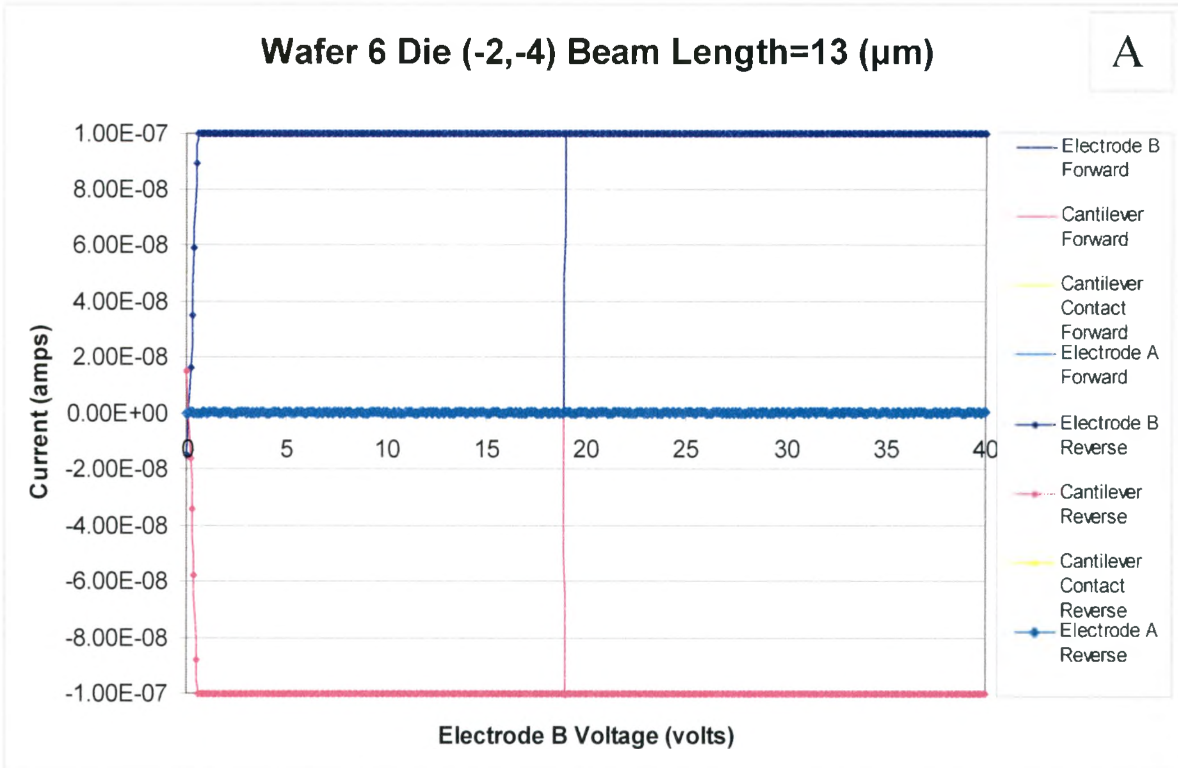

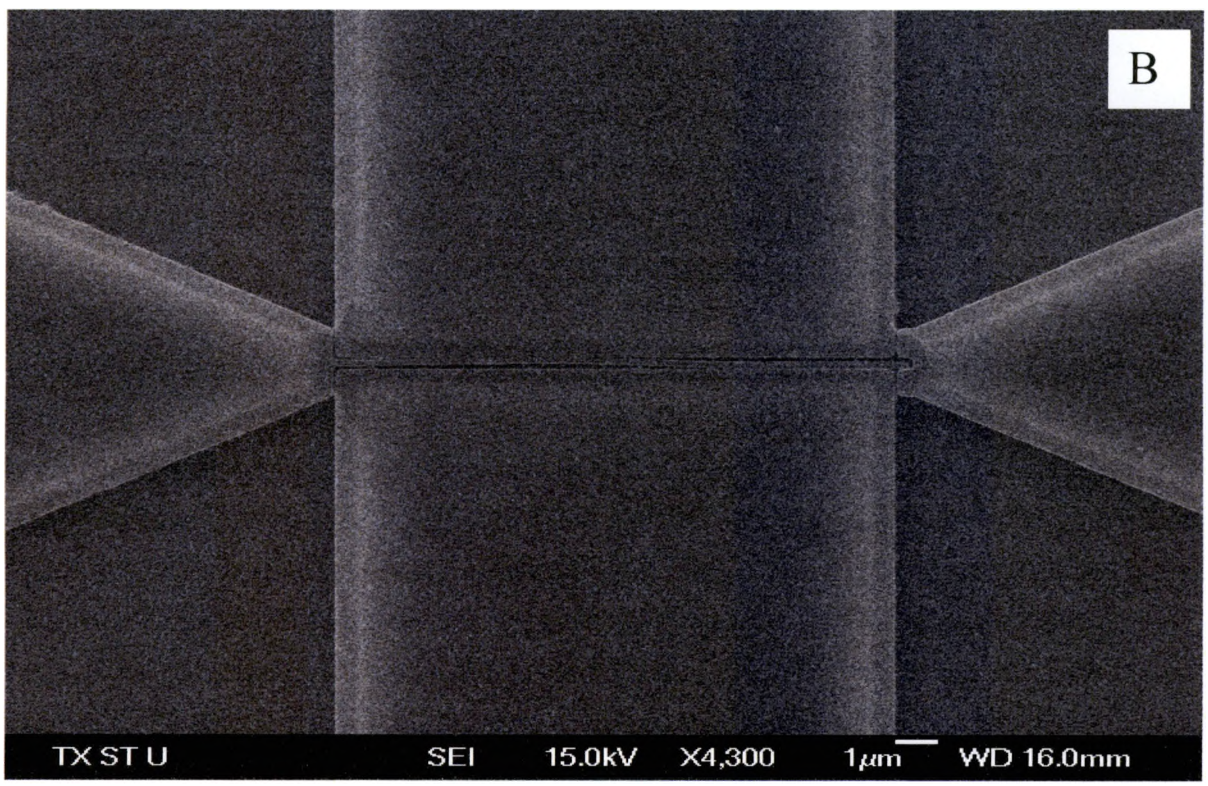

Fig. 3.14: Device displaying a switch and fusion of cantilever and electrode B.

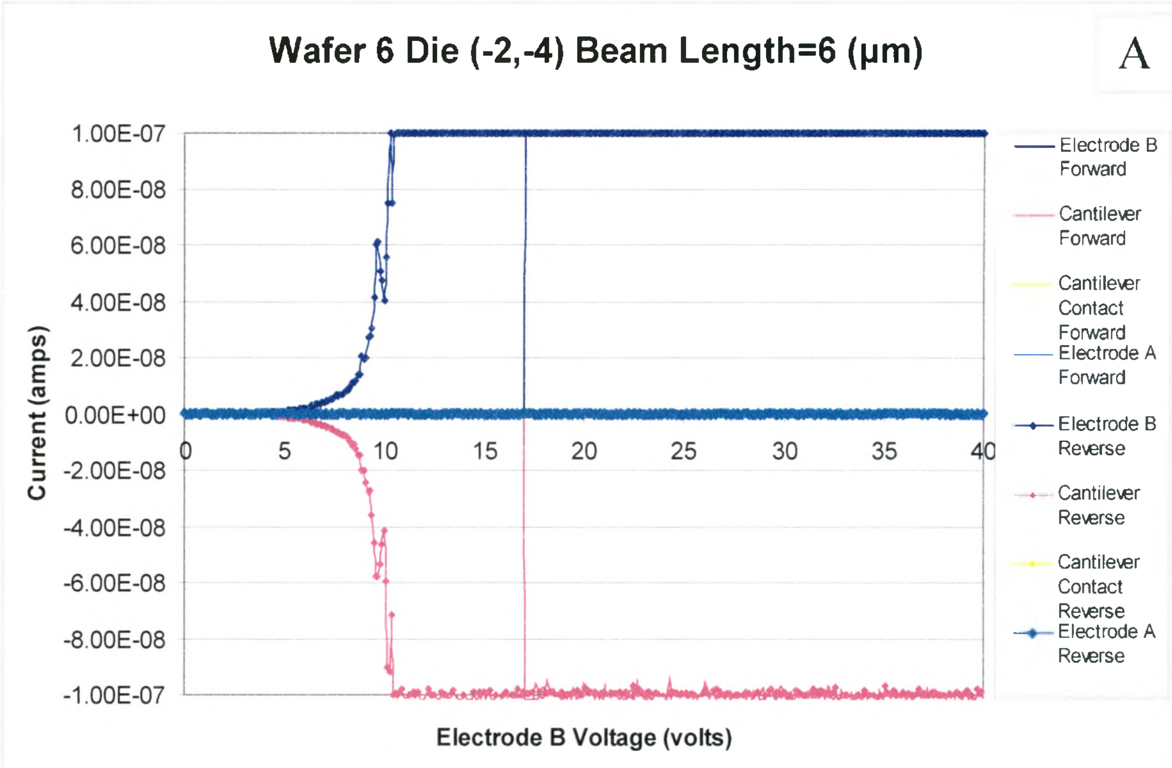

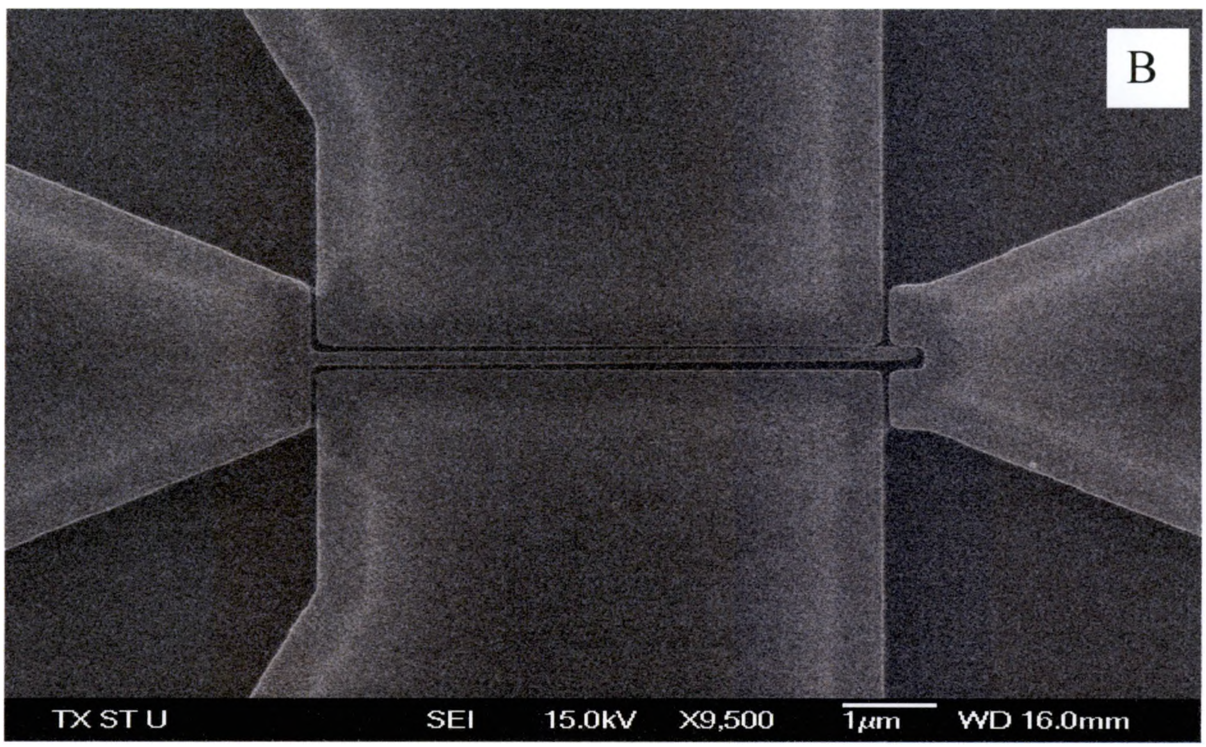

Fig. 3.15: Device displaying a switch and fused pull-out cantilever from electrode B.

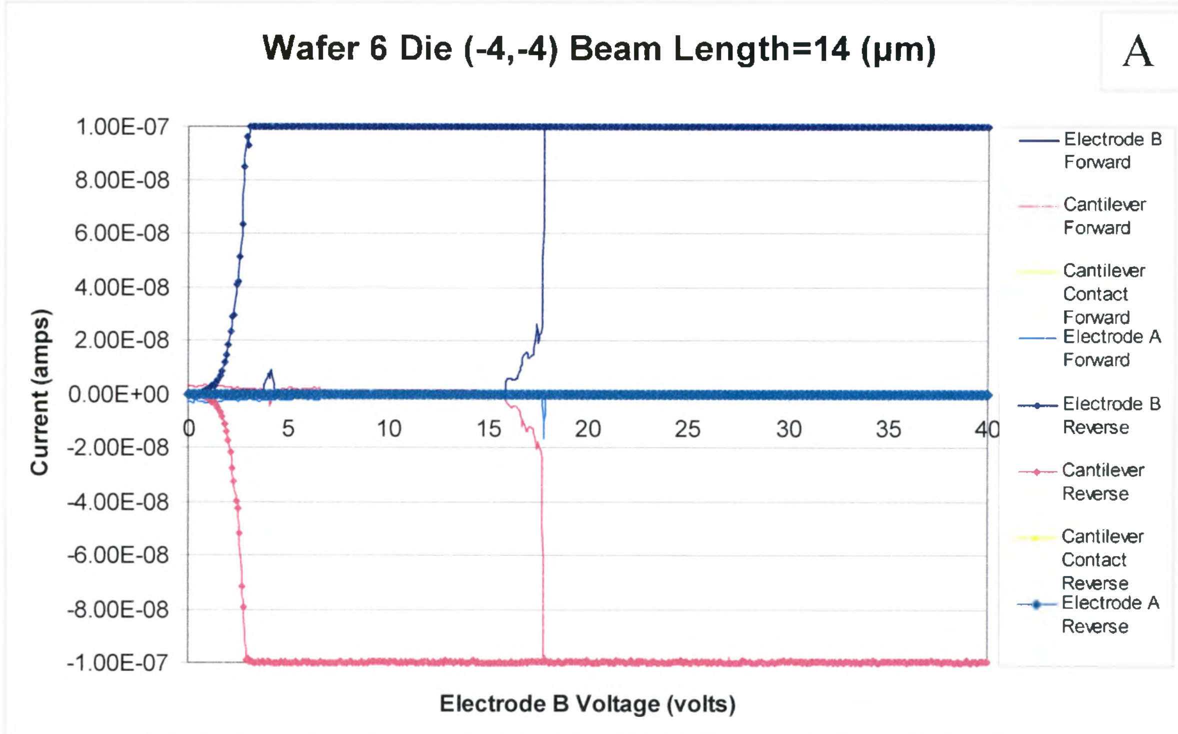

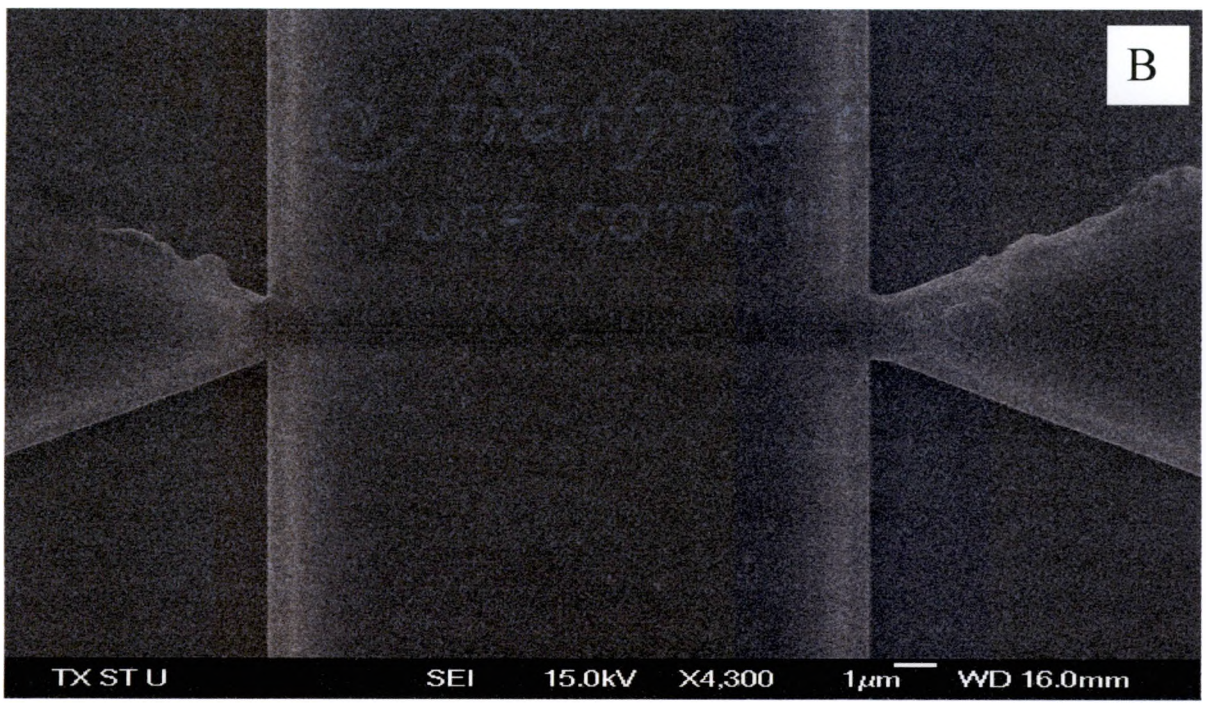

Fig. 3.16: Device displaying a switch, fusion and etch residue.

Simulation Results

From equation 9 the important design parameters were determined to be the spring constant, the area, the initial gap size, and the voltage being applied. These parameters were then simulated to determine their dependence on the applied voltage and length of the cantilever. The following is how the parameters in this application alter the parameters in equation 9. The length and vertical thickness of the cantilever will affect the electrode and contact areas. The width, thickness, and length of the cantilever affect the resistance to bending or its spring constant. Finally the electrode gap affects the voltage to actuate the device, and the Young's modulus of the cantilever material controls the spring constant. The simulated pull-in voltages can be seen in comparison to the pull-in voltages predicted by equation 9 in Fig. 3.17. The reason that the simulated pull-in voltages are higher than the predicted pull-in voltages (equation 9) is because one end of the beam is fixed in the simulation, whereas the entire beam is free to move in the derivation of equation 9. The simulated results seen in Figs. 3.18-3.21 give values for the pull-in voltage that are of the same order of magnitude to the actual electrical data. However, the simulated pull-in values (the blue lines represent the physical device's design parameter) do not trend with the actual pull-in values measured. Part of the reason for this is that the simulations use the dimensions of the device as drawn on the mask set, not the actual dimensions after processing. Another reason could be that the simulations did not include the Ti-N layer, which would increase the width and stiffness of the cantilever while decreasing the gap size. This would shift the simulated pull-in values up on the graph, but it is still difficult to make a meaningful comparison between the simulated and experimental data due to the large variance across the wafer.

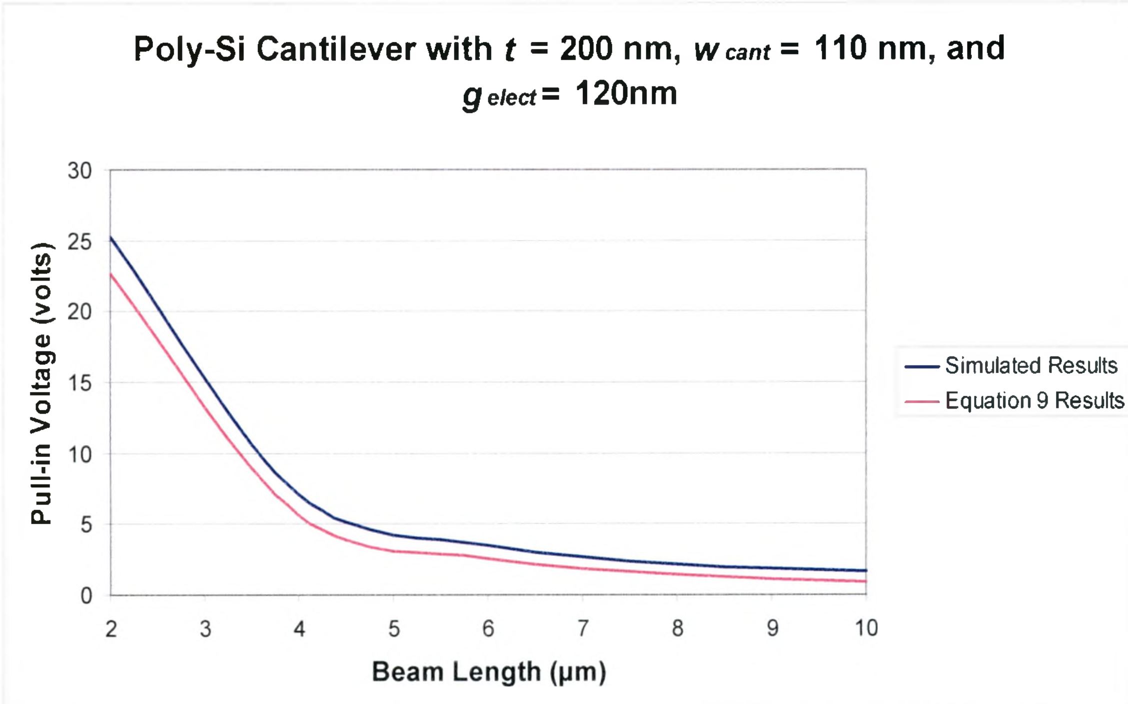

Fig. 3.17: Simulated pull-in voltage vs. equation 9 predicted pull-in voltage.

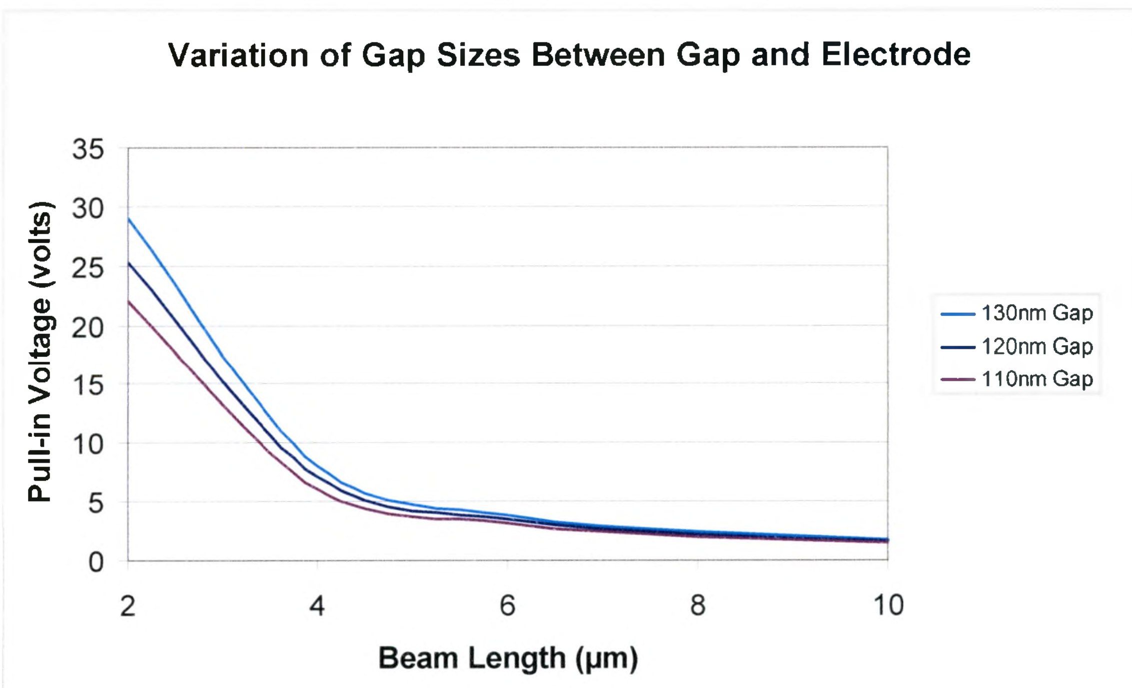

Fig. 3.18: Simulated pull-in voltage as a function of length for various gap sizes.

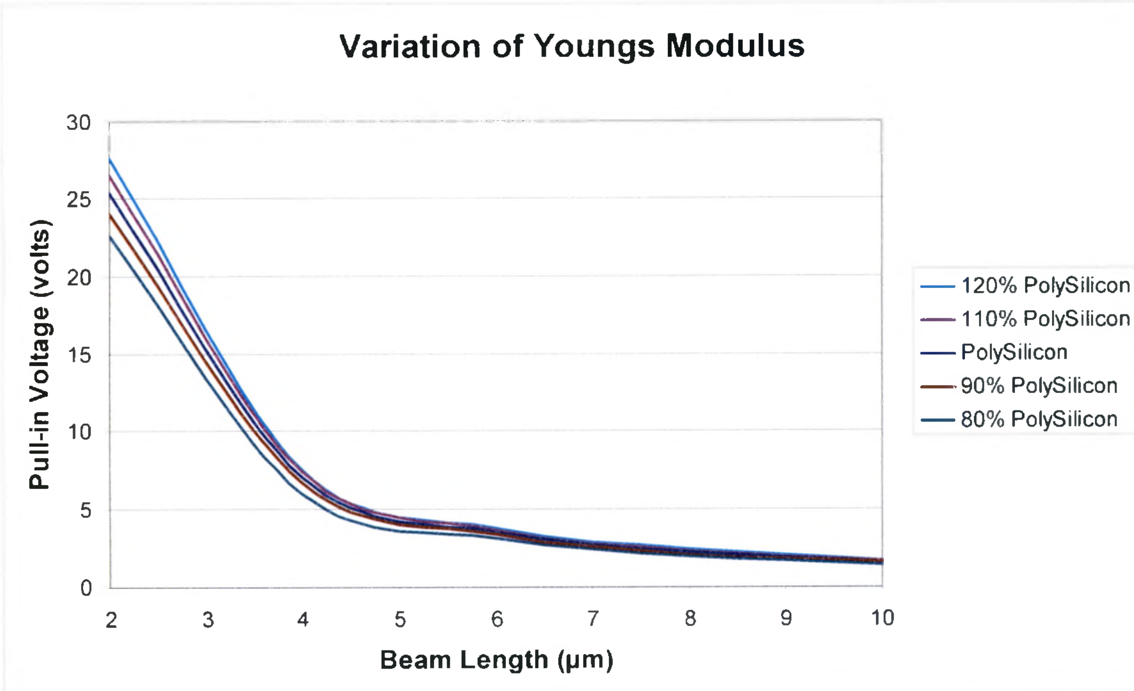

Fig. 3.19: Simulated pull-in voltage as a function of length for various Young's modulus.

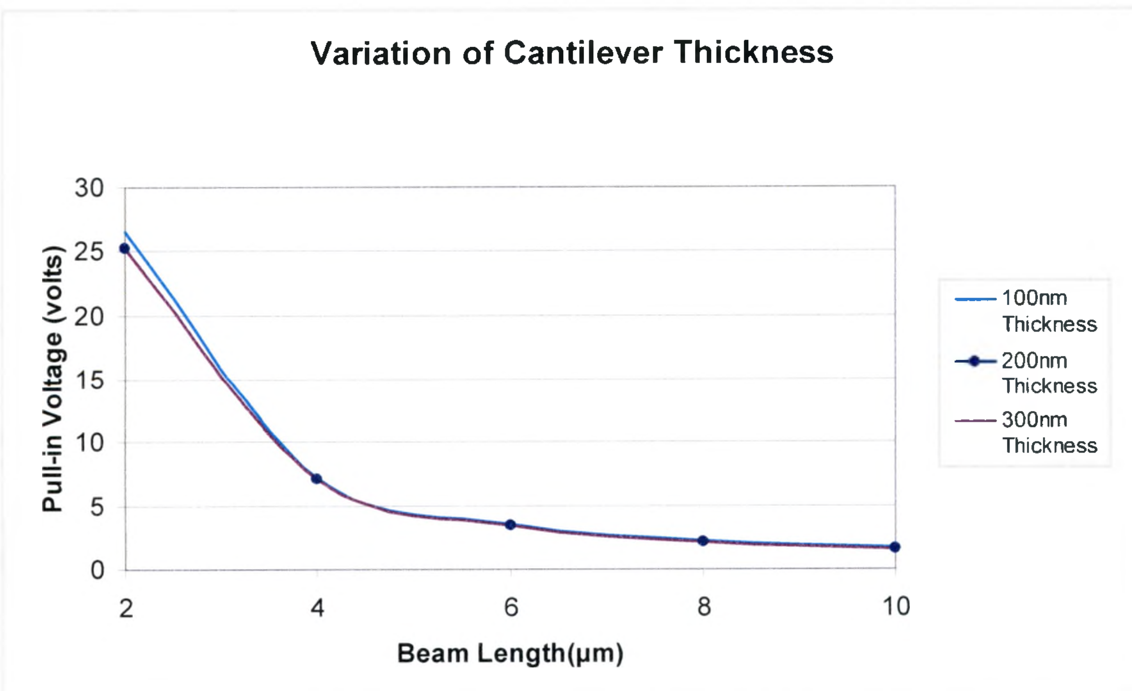

Fig. 3.20: Simulated pull-in voltage as a function of length for various thicknesses.

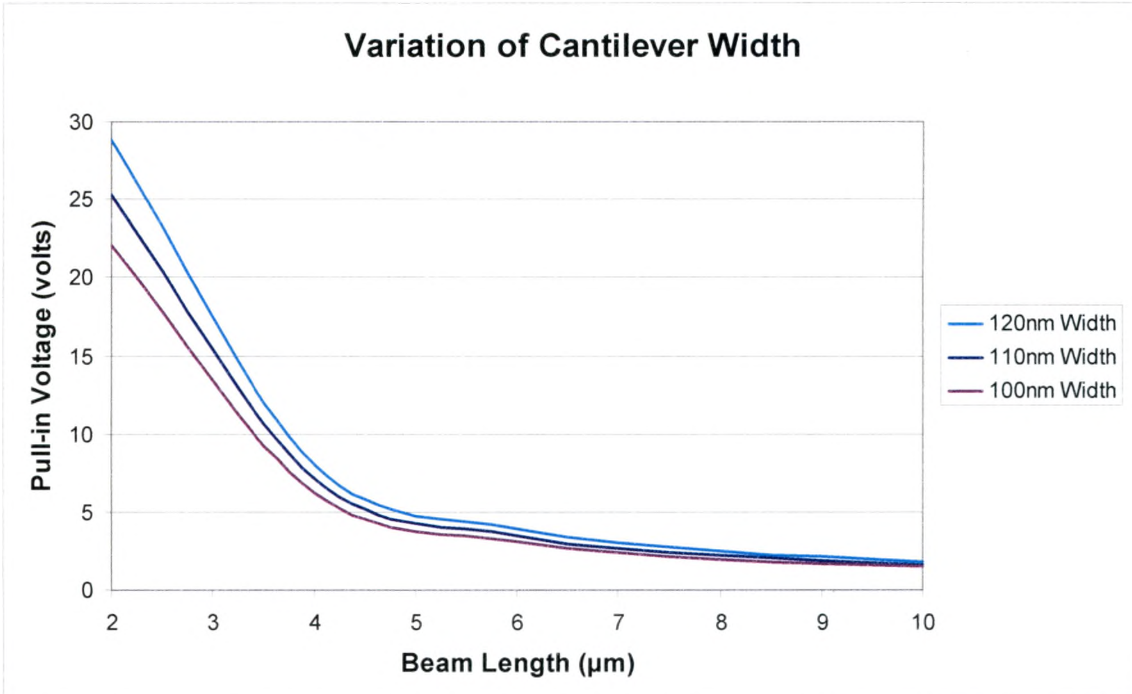

Fig. 3.21: Simulated pull-in voltage as a function of length for various widths.

Because of the large parasitic capacitance from the probe pads and the fact that most of the devices broke after one usage, it was not possible to test the switching speed of these devices. To estimate the natural frequency of oscillation, the analytic expression for the frequency of each mode of a cantilever was used

$$\omega_n = \frac{\alpha_n^2}{2\pi}\sqrt{\frac{EI}{mL^3}}\ , \qquad [18]$$

where α_n^2 represents the bending mode (seen in Fig 3.22) and m is the mass of the cantilever.[12]

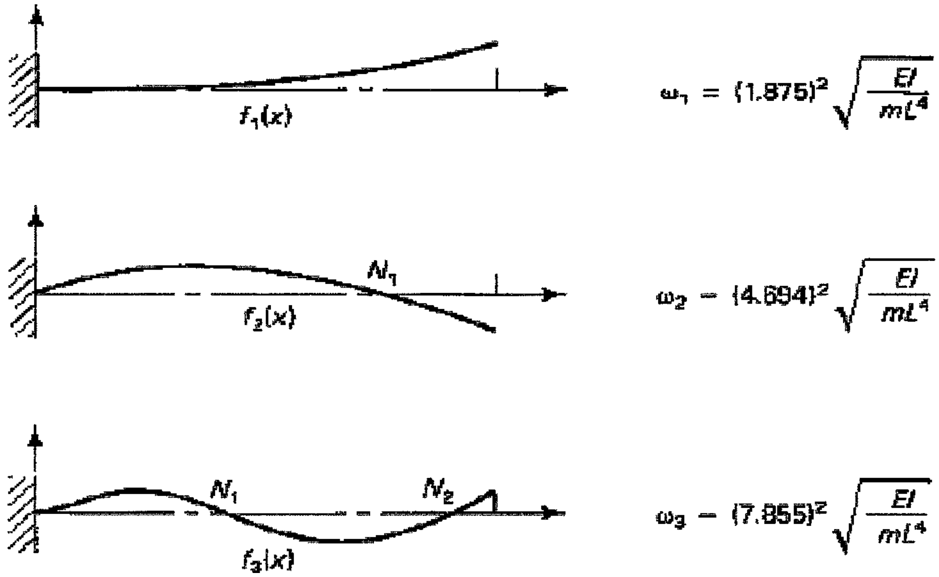

Fig. 3.22: Bending modes for cantilever beam.[13]

From this equation, a curve for the natural frequency of the first mode of the cantilever structure as a function of beam length was created, as seen in Fig. 3.23. The frequency of the device is important because it has a direct correlation with how fast the computations or data storage can be made using the cantilevers.

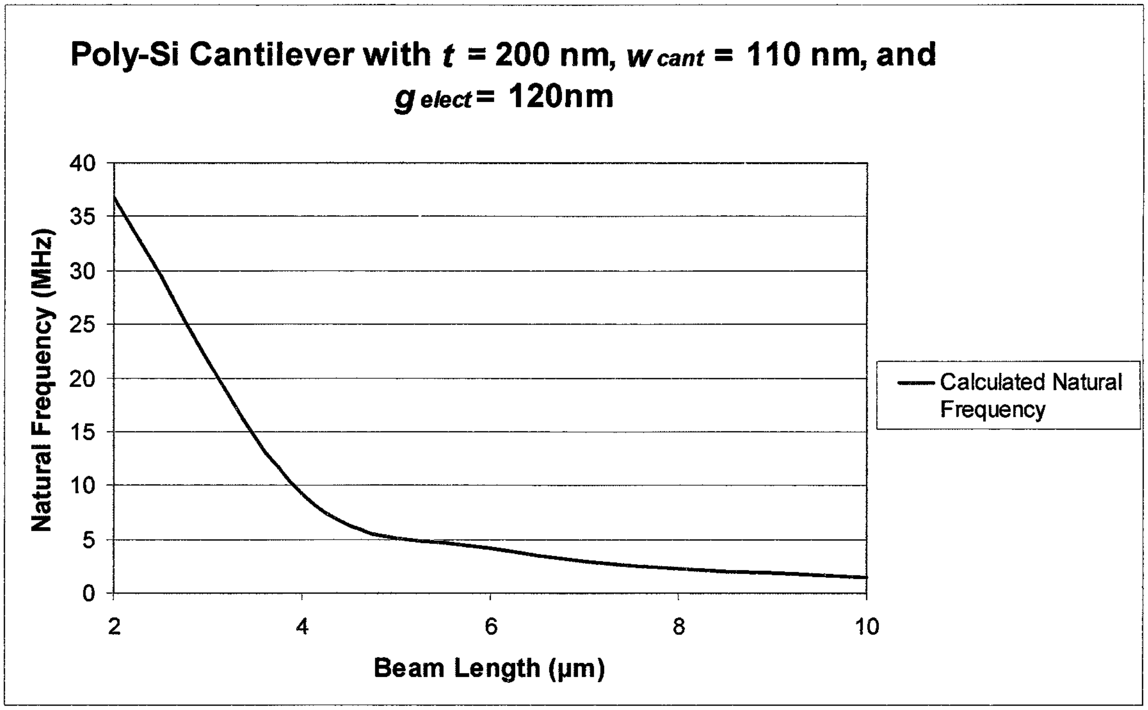

Fig. 3.23: Natural frequency as a function of beam length.

To enhance the performance and reliability of the cantilever devices, slight alterations of the cantilever design are currently being investigated. First, the overlap between the cantilever and the cantilever contact is being increased. This ensures a low resistance contact between the two and also that the cantilever does not contact the high voltage driving electrode, which often results in a short with the current design. In addition, by fixing the cantilever contact and eliminating possible electrode shorts, a new test of the device lifetime of the device can be done to determine the number of cycles possible for various materials. Second, adding in a remote metal layer for the contacts will reduce the parasitic capacitance and allow the time dependant analysis of the cantilevers. This will provide an experimentally determined speed of the device that can be compared with the theoretical one. Additionally, a serpentine spring section was added near the base of the cantilever to decrease the spring constant and help lower the pull-in voltage even more. Decreasing the gap size of the cantilever contact compared to the electrode gap size was also done to help ensure that the end of the cantilever connects with the cantilever contact terminal instead of the electrode. These changes can be seen in Fig. 3.24.

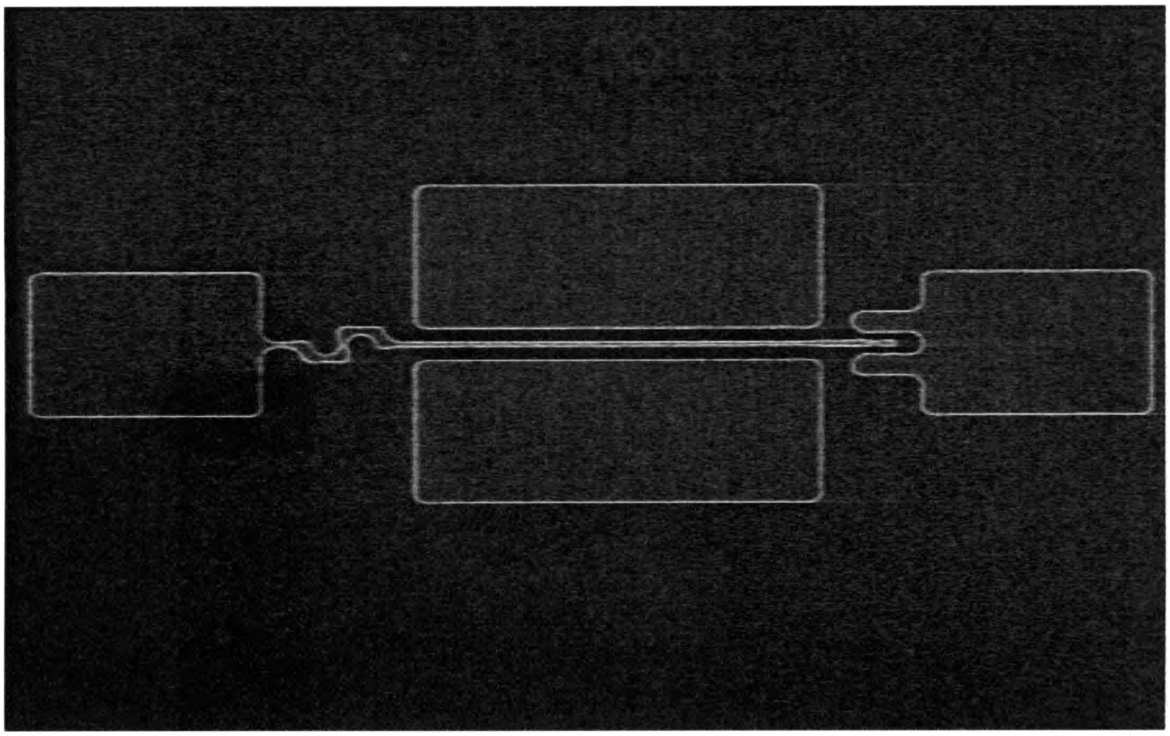

Fig. 3.24: SEM image of altered NEMS cantilever design provided by SEMATECH.

Further tweaks to the process in regards to the optical proximity correction could be done to create a device with square edges as well as control the size of the width of the cantilever at its base and increase the width of the cantilever near the cantilever contact. This would help to further decrease the pull-in voltage and mechanical delay.

CHAPTER 4

CONCLUSIONS

The operating parameters and failure mechanisms of poly-Si NEMS cantilever relays were investigated via four point probe analysis, imaging with SEM, and simulation with COMSOL. From these tests it was found that the variation across a wafer played a larger effect on the pull-in voltage than the length of the cantilever. In addition, shorts between the cantilever and driving electrodes are the most common failures. These failures either happened due to processing variations across the various wafers or due to electrical fusing during device operation. Even though most of the devices shorted when they switched on, there were still a few devices that went through multiple cycles, demonstrating the possibility of the device being used as a logic element. The SEM images confirmed the fusing of the cantilever to the different terminals, but did not help answer why some of the devices had higher pull-out voltages than pull-in voltages. Finally, the simulation results confirmed that the validity of using equation 9 to determine the dependence of the pull-in voltage on the various device parameters. The simulations also showed that the three features that have the largest effect on the pull-in voltage are the cantilever length, cantilever width, and electrode gap spacing. The natural frequencies for this device also show that the device is capable of most RF applications but is not fast enough to compete with CMOS transistor technology. Some of the mechanics of the NEMS cantilever relay learned in this study will help in the redesign of the device and could result in the development of relays that start to approach the desired traits of a logic device (low power, low voltage, small footprint, and fast switching speed).

REFERENCES

[1]J.J. Allen, *Micro Electro Mechanical System Design* (Taylor & Francis Group, Florida, 2005).

[2] S.D. Senturia, *Microsystem Design* (Springer Science+Business Media, Inc., New York, 2001, p. 125-138).

[3] S.D. Senturia, *Microsystem Design* (Springer Science+Business Media, Inc., New York, 2001, p. 130).

[4] S.D. Senturia, *Microsystem Design* (Springer Science+Business Media, Inc., New York, 2001, p. 129).

[5]N.R. Bauld, Jr., *Mechanics of Materials* (Wadsworth, Inc., California, 1982, p. 342-343).

[6]N.R. Bauld, Jr., *Mechanics of Materials* (Wadsworth, Inc., California, 1982, p. 342.)

[7] J. Simon, S. Saffer, F. Sherman, and C. Kim, Lateral Polysilicon Microrelays with a Mercury-Drop Contact, Mechanical and Aerospace Engineering Department, University of California, California, 1998.

[8] L.L. Mercado, S. Kuo, T.T. Lee, and R. Lee, *Process-Induced Thermal Effects on Packaging Yield of RF MEMS Switches* (ASME, Louisiana, 2002).

[9] F. Djuth, *Memes RF Switches with Ultra-Higher Switching Speeds*, (GeoSpace Research, INC., California).

[10] D.M. Geetha and M. Madheswaran, *Optical MEMS Electrostatic Actuators with various Beam Configurations*, proceedings of the International Conference on Microwave, 2008 pp. 757-760.

[11] D.K. Schroder, *Semiconductor Material and Device Characterization: Third Edition* (John Wiley & Sons, Inc., New Jersey, 2006, p. 629-634).

[12] S. S. Rao, *Mechanical Vibrations*: 4th edition, Pearson Edition, (Prentice Hall, New Jersey, 2003, p. 609 – 613).

[13] Faculty, Mechanical Engineering Department, University of Massachusetts, Lowell, *Cantilever Beam Experiment* (unpublished).

VITA

Jason L. Williams was born April 21, 1983 to Ellen Williams in Tucson, Arizona. He has an older brother James and younger sister Rachel. He moved to Austin, Texas in 1994. He later attended Austin High School where he graduated in 2001. After graduation Jason attended Texas State University-San Marcos. He was awarded a Bachelor of Science in Physics in May 2006. In August 2006 he attended Oregon State University with a major in Nuclear Engineering. In Fall 2007 he transferred to Texas State University-San Marcos and switched majors from Nuclear Engineering to Material Physics. He began studying NEMS at his internship at SEMATECH June 2008 through January 2009.

Permanent Address: someid_123@yahoo.com

This thesis was typed by Jason L. Williams.